ACS Catalysis

Research Article

pubs.acs.org/acscatalysis

Role of Branching on the Rate and Mechanism of C–C Cleavage in Alkanes on Metal Surfaces

David D. Hibbitts,[†,∥] David W. Flaherty,[†,§] and Enrique Iglesia*[,†]

[†]Department of Chemical and Biomolecular Engineering, University of California, Berkeley, California 94720, United States

[∥]Department of Chemical Engineering, University of Florida, Gainesville, Florida 32611, United States

[§]Department of Chemical and Biomolecular Engineering, University of Illinois at Urbana–Champaign, Urbana, Illinois 61801, United States

Supporting Information

ABSTRACT: The kinetic relevance and rates of elementary steps involved in C–C bond hydrogenolysis for isobutane, neopentane, and 2,3-dimethylbutane reactants were systematically probed using activation enthalpies and free energies derived from density functional theory. Previous studies showed that C–C cleavage in alkanes occurs via unsaturated species formed in fast quasi-equilibrated C–H activation steps, leading to rates that decrease with increasing H_2 pressure, because of a concomitant decrease in the concentration of the relevant transition states. This study, together with previous findings for *n*-alkanes, provides a general mechanistic construct for the analysis and prediction of C–C hydrogenolysis rates on metals. C–C cleavage in alkanes is preceded by the loss of two H atoms and the formation of two C-metal (C–M) bonds for each ^{1}C and ^{2}C atom involved in the C–C bond. Metal atoms transfer electrons into the ^{1}C and ^{2}C atoms as C–C bonds cleave and additional C–M bonds form. ^{3}C and ^{4}C atoms of isobutane, neopentane, and 2,3-dimethylbutane, however, do not lose H atoms before C–C cleavage, and thus, transition states cannot bind the ^{3}C and ^{4}C atoms in the C–C bond being cleaved to surface metal atoms. C–H activation occurs instead at ^{1}C atoms vicinal to the C–C bond, which lose all H atoms and form three C–M bonds. These transition states involve electron transfer into the metal surface, leading to a net positive charge at the ^{3}C and ^{4}C atoms; these atoms exhibit sp^2 geometry and resemble carbenium ions at the C–C cleavage transition state, in which they are not bound to the metal surface. These mechanistic features accurately describe measured H_2 effects, activation enthalpies, and entropies, and furthermore, they provide the molecular details required to understand and predict the effects of temperature on hydrogenolysis rates and on the location of C–C bond cleavage within a given alkane reagent. The result shown and the conclusions reached are supported by rigorous theoretical assessments for C–C cleavage within about 200 intermediates on Ir surfaces, and the results appear to be applicable to other metals (Rh, Ru, and Pt), which show kinetic behavior similar to Ir.

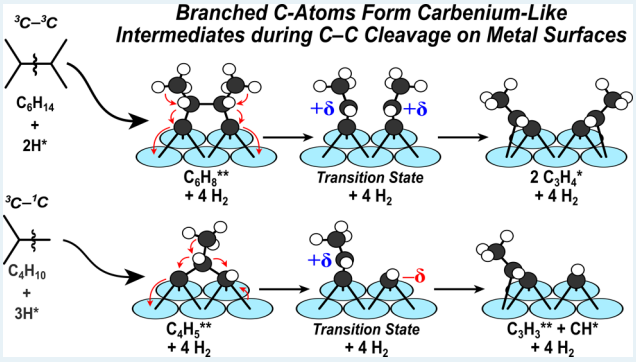

KEYWORDS: *hydrogenolysis, alkane activation, metal catalysis, density functional theory, kinetics*

1. INTRODUCTION

Metal-catalyzed C–C hydrogenolysis is used to decrease the chain length of acyclic alkanes and to open cycloalkane rings;[1−6] it is also an undesired side reaction in reforming and isomerization processes.[7−9] The relative rates of C–C rupture in substituted and unsubstituted C–C bonds of alkanes depend on temperature and H_2 pressure, as well as on the identity and size of metal particles.[2−6,9−11] The reactive intermediates involved and the activation energies for C–C rupture depend also on the degree of branching at the C atoms involved in the cleaved C–C bond.[2−6,9−11] C–C activation occurs after extensive dehydrogenation of the reactant alkanes,[12−18] a process that weakens C–C bonds on catalyst surfaces by replacing C–H bonds with C–M bonds (where M is a surface metal atom) and concomitantly placing electrons in antibonding orbitals of C–C bonds.[19,20] These dehydrogenations also form H_2 (from H* recombination) that increases activation entropies and lower activation free energies (thus increasing rates). The structure and H-content of the reactive intermediates involved, however, can only be inferred indirectly from the effects of H_2 pressure on C–C rupture rates,[13−15,21] because such species exist at low surface concentrations during catalysis, making them inaccessible to spectroscopic probes. As a result, their identity and structure can be discerned only through theoretical methods.[22−29]

Received: September 2, 2015
Revised: November 19, 2015
Published: December 18, 2015

DOI: 10.1021/acscatal.5b01950
ACS Catal. 2016, 6, 469−482

Previous theoretical studies on *n*-alkanes[22,23] and methylcyclopentane[26−28] concluded that bonds containing only primary (^{1}C) and secondary (^{2}C) C atoms cleave via *α,β*-bound RC*C*R′ intermediates (where * indicates the previous C atom is bound to the surface). The extensive dehydrogenation that occurs before forming these transition states is consistent with the strong inhibition effects of H_2 on alkane hydrogenolysis reactions.[10,13−15,22−24,30−36] For example, turnover rates for hydrogenolysis of ^{1}C−^{1}C bonds in ethane are proportional to $(H_2)^{-3}$ ((H_2) denotes H_2 pressure) on H*-saturated Ir surfaces;[22,30] a similar exponent was reported for cleaving ^{2}C−^{1}C and ^{2}C−^{2}C bonds in longer *n*-alkanes,[30] branched alkanes,[10] and cycloalkanes.[10,36] Their similar H_2 dependences[10,22,33,36] suggest that C−C bonds with only ^{1}C and ^{2}C atoms cleave via *α,β*-bound RC*−C*R′‡ transition states (indicated by the ‡ symbol) resembling those proposed to mediate the hydrogenolysis of methylcyclopentane[26−28] and ethane.[22] Recent theoretical studies[23] on propane and butane have confirmed that these *n*-alkanes also cleave via *α,β*-bound RC*−C*R′‡ transition states (as was observed for ethane[22]).

The hydrogenolysis of C−C bonds containing one or more tertiary carbon atoms (^{3}C−^{x}C) exhibits higher activation enthalpies and entropies than for C−C bonds with only ^{1}C and ^{2}C carbons.[10] These ^{3}C−^{x}C cleavage rates also are more strongly inhibited by H_2 ($r \sim (H_2)^{-(4-4.5)}$) than for ^{2}C−^{2}C cleavage ($r \sim (H_2)^{-3}$), even though the C atoms in the ^{3}C−^{x}C bonds being cleaved contain fewer H atoms. These findings suggest that ^{3}C−^{x}C bonds cleave only after the additional activation of C−H bonds at C atoms away from the C−C being cleaved.[10] These data contradict previous proposals based on theoretical treatments that concluded that ^{3}C−^{2}C bonds in methylcyclopentane cleave via *α,β*-bound intermediates that are less dehydrogenated than those involved in ^{2}C−^{2}C cleavage in *n*-alkanes and methylcyclopentane.[26−28] It seems implausible that *α,β*-bound intermediates are required for all C−C cleavage reactions, because such structures cannot explain the rupture of ^{4}C−^{x}C bonds, such as the ^{4}C−^{1}C bonds in neopentane, for which the ^{4}C atom remains coordinatively saturated and cannot bind onto metal surfaces prior to C−C cleavage. Thus, neopentane hydrogenolysis must proceed via metallacyclic (i.e., *α,γ*- or *α,γ,δ*-bound) intermediates that undergo subsequent C−C cleavage. Both *α,γ*- and *α,δ*-bound metallacycles have been inferred from isotopic exchange measurements during alkane hydrogenolysis (of linear and branched species),[9,12,37−42] but their involvement as intermediates in C−C cleavage reactions remains unconfirmed by theoretical study.

Here, we use density functional theory calculations (DFT) to systematically examine the cleavage of C−C bonds in isobutane, neopentane, and 2,3-dimethylbutane (Scheme 1), including C−C activation in *α*- and *α,β*-bound intermediates, *α,γ*- and *α,δ*-bound metallacyclic intermediates, and intermediates with 3−4 C atoms bound to the surface (*α,β,γ*-, *α,β,δ*-, *α,γ,δ*-, and *α,β,γ,δ*-bound intermediates). Through contrast with previous studies on *n*-alkane activations of ethane, propane, and butane, we are able to demonstrate the effects of methyl-substitution on C−C cleavage mechanisms. We find that ^{3}C−^{x}C bonds in isobutane and 2,3-dimethylbutane activate via *α,γ*- and *α,δ*-bound intermediates that form via dehydrogenation at ^{1}C atoms not involved in the ^{3}C−^{x}C bond being cleaved. These findings contrast the *α,β*-bound species involved in cleaving C−C bonds with only ^{1}C and ^{2}C (e.g., in *n*-alkanes), which involve dehydrogenation only at the C atoms in the cleaved C−C. The inability of ^{3}C−^{x}C bonds to bind their ^{3}C atoms (through C−H activations) to the extent required for C−C cleavage imposes enthalpy barriers that can only be compensated via the activation of C−H bonds at ancillary positions and the resulting entropic gains via the concomitant evolution of H_2 prior to the formation of the transition state.

Scheme 1. C−C Bond Activation Reactions Examined in This and Previous Studies,[22,23] Which Include *n*-Alkanes Containing C−C Bonds Composed of Only Primary (^{1}C) and Secondary (^{2}C) C Atoms, and Branched Alkanes Containing Tertiary (^{3}C) and Quaternary (^{4}C) C Atoms

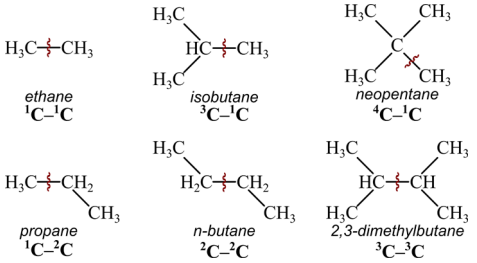

2. METHODS

2.1. Computational Methodology and Catalyst Models. Periodic plane-wave density functional theory (DFT) calculations were performed using the Vienna *ab initio* simulation package (VASP)[43−46] as reported elsewhere.[22,23] Plane waves were constructed using projector augmented-wave (PAW) potentials with an energy cutoff of 396 eV.[47,48] The revised Perdew−Burke−Ernzerhof (RPBE) form of the generalized gradient approximation (GGA) was used to determine exchange and correlation energies.[49−51] Select calculations were repeated with the (nonrevised) PBE functional and showed that the conclusions herein were not dependent upon the revisions made in the RPBE functional (Figure S1, Supporting Information, SI). Wave functions were converged to within 10^{-6} eV and forces were computed using a fast Fourier transform (FFT) grid with a cutoff of twice the planewave cutoff. A 3 × 3 × 1 Monkhorst-pack sampling of the first Brillouin zone (k-point mesh) was used.[52] Structures were relaxed until all forces on unconstrained atoms were <0.05 eV/Å. After geometric convergence, single-point calculations with a 6 × 6 × 1 k-point mesh were performed to estimate the energies of the reactants, products, and transition states.

The energies of gaseous species were calculated by placing them in 18 × 18 × 18 Å unit cells. The Ir(111) surface was modeled as a 4 × 4 lattice using an experimentally measured lattice parameter of 3.84 Å.[53] Four layers were present in the *z*-direction (orthogonal to the (111) surface); the bottom two layers were fixed in their bulk positions, and the other two were relaxed to their minimum energy locations.

Transition-state structures were obtained for each elementary reaction using dimer[56] methods which were initialized by nudged elastic band (NEB)[54,55] methods. NEB calculations were carried out using 16 images, and wave functions were converged to within 10^{-4} eV using a 3 × 3 × 1 k-point mesh and a FFT grid size of 1.5 times the planewave cutoff. The maximum force on each atom was converged to <0.3 eV/Å. These NEB calculations provide an estimate of the reaction path and a starting point for the structure and the mode along the reaction coordinate for each transition state. The dimer algorithm was then used with wave functions converged to

DOI: 10.1021/acscatal.5b01950
ACS Catal. 2016, 6, 469−482

within 10^{-6} eV using a 3 × 3 × 1 k-point mesh and an FFT grid size of two times the planewave cutoff. For dimer calculations, the maximum force on each atom was converged to <0.05 eV Å^{-1}. As in the case of the optimization of reactant and product states, the energy of the transition state was determined using a single-point calculation with 6 × 6 × 1 k-point mesh. Vibrational frequency calculations confirmed the presence of a single imaginary mode for all transition states studied herein.

Frequency calculations were performed on all optimized states to determine zero-point vibrational energies (ZPVE), vibrational enthalpies (H_{vib}), and free energies (G_{vib}). These terms were then used, together with electronic energies (E_0, provided by VASP), to estimate enthalpies:

$$H = E_0 + \mathrm{ZPVE} + H_{vib} + H_{trans} + H_{rot} \quad (1)$$

and free energies:

$$G = E_0 + \mathrm{ZPVE} + G_{vib} + G_{trans} + G_{rot} \quad (2)$$

for all reactants, products, and transition states at 593 K (the temperature at which H_2 dependence was studied for isobutane and 2,3-dimethylbutane[10]). For gaseous molecules, translational and rotational enthalpies and free energies were also computed from statistical mechanics. Equations for ZPVE, H_{vib}, and G_{vib} from vibrational frequencies and H_{trans}, H_{rot}, G_{trans}, and G_{rot} for gas-phase molecules are reported in the SI (eqs S1−S11). The sum of these corrections in eqs 1 and 2 are used throughout to determine the enthalpies and free energies of all states (including transition states).

The RPBE functional used lack any terms for dispersive interactions, leading to overestimates of activation enthalpies and free energies for the C−C cleavage reactions reported herein. The differences between barriers for similarly sized transition states, which matter in assessing the relative contributions of competing routes, are, however, unlikely to be altered by the inclusion of such dispersive interactions, because they differ only in the number of H atoms which contribute very weakly to dispersive interactions. It is such differences that lead to the presented conclusions about the preferred routes for C−C cleavage in isobutane, neopentane, and 2,3-dimethylbutane.

DFT-derived intrinsic enthalpy and free energy barriers (ΔH_{act} or ΔG_{act}, respectively) denote differences in enthalpy or free energy between a transition state and the precursor reactant for that elementary step. Reaction enthalpies and free energies (ΔH_{rxn} or ΔG_{rxn}, respectively) denote differences between the products and reactants for an elementary step.

2.2. Mechanistic Connections between Measured Rate and DFT-Derived Reaction Energetics. Scheme 2 shows a sequence of steps that leads to the cleavage of C−C bonds in alkanes. These steps lead to a rate equation that accurately described the effects of alkane and H_2 pressure on the hydrogenolysis rates of ethane,[13−15,22,23,29−31] larger *n*-alkanes (C_3−C_{10}),[30,32−34] branched alkanes (C_4−C_6),[10,32,35] and alkyl cyclohexanes.[10,36] Equilibrated mixtures of alkanes and their unsaturated homologues (alkenes, arenes) indicate that dissociative H_2 adsorption (2.1), alkane adsorption (2.2), alkane dehydrogenation (2.3), and alkene desorption steps are all quasi-equilibrated during alkane hydrogenolysis on Ir, Ru, Rh, and Pt clusters.[10,22,30,36] C−C bond cleavage occurs within partially dehydrogenated intermediates ($C_nH^{l*}_{m-y}$)[12−18] which bind to *l* number of sites all which are quasi-equilibrated with the gaseous alkane reactants.

Scheme 2. Mechanism for Alkane Hydrogenolysis on Metal Catalysts[a]

$$H_2 + 2* \overset{K_{H_2}}{\rightleftharpoons} 2\,H^* \quad (2.1)$$

$$C_nH_m + * \overset{K_{C_n}}{\rightleftharpoons} C_nH^*_m \quad (2.2)$$

$$C_nH^*_m + (l-1)* \overset{K_{CH,y}}{\rightleftharpoons} C_nH^{l*}_{m-y} + 0.5y\,H_2 \quad (2.3)$$

$$C_nH^{l*}_{m-y} \xrightarrow{k_{CC,y}} C_aH^{c*}_b + C_{n-a}H^{d*}_{m-y-b} \quad (2.4)$$

$$C_aH^{c*}_b + x\,H^* \rightleftharpoons C_aH_{2a+2} + (c+x)* \quad (2.5)$$

[a] $\rightleftharpoons$ denotes a quasi-equilibrated reaction, * an unoccupied surface site; *l** an adsorbate occupying *l* surface sites, K_x and k_x are equilibrium and rate constants for individual steps.

C−C bond cleavage occurs in these partially dehydrogenated intermediates at rates described by

$$\frac{r_y}{[L]} = k_{CC,y}[C_nH^{l*}_{m-y}] \quad (3)$$

where $r_y/[L]$ is the turnover rate (i.e., rate normalized by exposed metal atoms [L]), $k_{CC,y}$ is the C−C cleavage rate constant for an intermediate that has undergone *y* C−H activations, *l* is the number of sites required for the transition state that mediates the C−C cleavage of that intermediate. Chemisorbed hydrogen atoms (H*) are the most abundant surface intermediate (MASI) at high H_2:C_nH_m ratios (>100), as shown by hydrogenolysis rates that depend linearly on alkane pressure and inversely on H_2 pressure for C_2−C_{10} *n*-alkanes, C_4−C_6 branched alkanes, and alkyl cyclohexanes.[10,22,30,36] The pseudo steady-state hypothesis for $C_nH^l*_{m-y}$ on the H*-saturated surface then leads to the rate equation:

$$\frac{r_y}{[L]} = k_{CC,y}\frac{(\prod_y^{i=1} K_{CH,i})K_{C_n}(C_nH_m)}{(K_{H_2}H_2)^{\lambda}} \quad (4)$$

where the $(\prod_{i=1}^{y} K_{CH,i})$ term represents the product of the equilibrium constants for the *y* number of C−H activations that occur before C−C cleavage. The dependence of the rate on (H_2), given by λ, depends on the identity and size of the active metal clusters and on the degree of substitution at the C atoms in the C−C bond cleaved.[10] The value of λ equals the number of H_2(g) molecules evolved in forming the kinetically relevant transition state via rupture of *y* C−H bonds and desorption of *l* H* atoms (to free up sites on a H*-saturated Ir surface, this was referred to as γ in previous publications[10,22,30,36] by our group but is changed here to avoid ambiguity as γ is used to refer to the binding of a species at its third C atom); these steps are required to form the C−M bonds that bind the transition state to metal surfaces. Bond-order conservation then suggests that the value of λ equals:

$$\lambda = 1/2(y + l) \quad (5)$$

where *l* is the number of C atoms that bind to the surface during C−C cleavage.

Taken together, the thermodynamic foundations of transition-state theory and the quasi-equilibrated nature of steps

DOI: 10.1021/acscatal.5b01950
ACS Catal. 2016, 6, 469−482

2.1−2.3 dictate that gaseous alkanes and l H* atoms are quasi-equilibrated with the C−C cleavage transition state ($C_nH_ml^{\ddagger}$) and the λ H_2 molecules formed:

$$C_nH_m + l\,H^* \overset{K^{\ddagger}}{\rightleftharpoons} [C_nH_{m-y}^{l*}]^{\ddagger} + \lambda\,H_2 \quad (6)$$

where $K^{\ddagger}$ is the equilibrium constant for the formation of the transition state (and stoichiometric amounts of gas-phase H_2) from a gas-phase alkane and a H*-covered surface. Consequently, $K^{\ddagger}$ is related to the measured activation free energy ($\Delta G^{\ddagger}$) by

$$K^{\ddagger} = k_{CC,y}\frac{(\prod_y^{i=1} K_{CH,i})K_{C_n}}{(K_{H_2})^{\lambda}} = \frac{k_bT}{h}e^{(-\Delta G^{\ddagger}/RT)} \quad (7)$$

Here, $\Delta G^{\ddagger}$ denotes the sum of the reaction free energies (ΔG_{rxn}) for all intervening steps involved in forming the reactive intermediate that immediately precedes the formation of the transition state in the kinetically relevant step (from the gas-phase alkane and a H*-covered surface) and the intrinsic free energy barrier (ΔG_{act}) for the elementary step that cleaves the C−C bond.

For instance, ethane hydrogenolysis involves C−C activation within CH*CH*: this process requires the desorption of two H* atoms, the adsorption of C_2H_6, and the activation of C−H bonds to form the CH*CH* species that undergo C−C cleavage.[22] The $\Delta G^{\ddagger}$ value for this reaction include the adsorption free energies of H_2 ($\Delta G_{ads,H2}$, Step. 2.1) and C_2H_6 ($\Delta G_{ads,C2}$, Step. 2.2), the reaction free energies for four C−H activation steps that form CH*CH* from C_2H_6* ($\Sigma(\Delta G_{rxn,CH,i})$, Step. 2.3) and the intrinsic free energy barrier for C−C activation of CH*CH* ($\Delta G_{act,CC,2}$, Step. 2.4):

$$\Delta G^{\ddagger} = \Delta G_{act,CC,2} + \Sigma\Delta G_{rxn,CH,i} + \Delta G_{ads,C2} - 3\Delta G_{ads,H2} \quad (8)$$

Substituting the free energies of individual adsorbed and gas-phase species leads to

$$\Delta G^{\ddagger} = G[CH^* - CH^{*\ddagger}] + 3G[H_2(g)] - 2G[H^*] - G[C_2H_6(g)] \quad (9)$$

which does not depend on the free energies of any reactive intermediates. Analogous equations for $\Delta H^{\ddagger}$ and $\Delta S^{\ddagger}$ values through their relation to $\Delta G^{\ddagger}$:

$$\Delta G^{\ddagger} = \Delta H^{\ddagger} - T\Delta S^{\ddagger} \quad (10)$$

The general form of eq 9:

$$\Delta G^{\ddagger} = G[TS^{l*\ddagger}] + \lambda G[H_2(g)] - lG[H^*] - G[Alkane(g)] \quad (9a)$$

can be rewritten in terms of the free energy for dissociative H_2 adsorption ($\Delta G_{ads,H_2}$):

$$\Delta G^{\ddagger} = G[TS^{l*\ddagger}] + 0.5yG[H_2(g)] - 0.5l\Delta G_{ads,H_2} - G[Alkane(g)] \quad (11)$$

$\Delta G_{ads,H_2}$ was modeled by desorbing 2 H* as H_2 from H*-saturated Ir(111) surfaces (1 H*/Ir_{surf}) to give enthalpies and free energies for dissociative H_2 ($\Delta H_{ads,H_2} = -34$ kJ mol^{-1} and $\Delta G_{ads,H_2} = -10$ kJ mol^{-1}) consistent with high H* coverages at >500 kPa H_2.[22] Here, enthalpies and free energies of all states are obtained via eqs 1 and 2 (at 593 K, the temperature at which λ values were measured for isobutane and 2,3-dimethylbutane[10,22]). $\Delta H^{\ddagger}$ and $\Delta G^{\ddagger}$ values (and eqs 4 and 7) are then used to determine relative rates of C−C cleavage of intermediates derived from isobutane, neopentane, and 2,3-dimethylbutane, thus allowing theory to discriminate between C−C hydrogenolysis routes.

3. RESULTS AND DISCUSSION

3.1. Isobutane Hydrogenolysis. Isobutane has three equivalent $^3C-^1C$ bonds; these bonds rupture at rates described by eq 4, which also describes the hydrogenolysis rates of n-alkanes. Isobutane hydrogenolysis turnover rates are, however, more sensitive to H_2 pressure ($\lambda = 4.0 \pm 0.2$) than are rates for n-alkanes ($\lambda = 3.0 \pm 0.2$), indicating that their transition states require the removal of more hydrogen atoms from reactants (y) and/or from H*-saturated surfaces (l)[10] than those for n-alkane cleavage ($y = 4$, $l = 2$, $\lambda = 3$). The rupture of $^3C-^1C$ bonds in isobutane must proceed via C−C cleavage of an intermediate that differs from the α,β-bound (η^2, η^2) RC*C*R′ structures implicated for n-alkanes, because ^3C atoms contain, and therefore can lose, only one H atom and thus can form only one C−M bond. Here, we consider the energetics of C−C bond activation steps in the complete set of 80 distinct isobutane-derived intermediates, formed by dehydrogenation to form eight possible permutations of surface attachments (Figure 1).

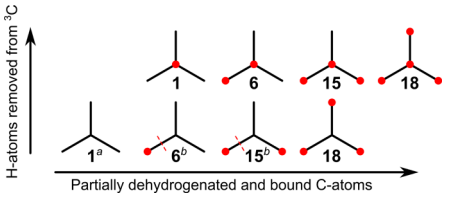

Figure 1. Forms of partially dehydrogenated isobutane intermediates organized by the total number of partially dehydrogenated C atoms and the number of H atoms (0 or 1) removed from the central ^3C. Dots indicate an attachment position where a C atom has lost one or more H atoms, and binds to the metal surface. Numbers near each structure indicate the number of different C−C cleavage transition states formed from intermediates with those surface attachments. [a]C−C cleavage within molecular isobutane not calculated. [b]Only C−C cleavage of partially dehydrogenated C−C bonds (indicated by dashed lines) was calculated.

C−C ruptures in α- and α,β-bound intermediates on Ir surfaces were considered by determining their effective enthalpy ($\Delta H^{\ddagger}$) and free energy ($\Delta G^{\ddagger}$) barriers using DFT; the latter are directly responsible for measured rate constants for C−C activation (eqs 4 and 7). C−C cleavage in $(CH_3)_2C^*CH^*$ mediated by $(CH_3)_2C^*-CH^{*\ddagger}$ exhibits the lowest $\Delta H^{\ddagger}$ (224 kJ mol^{-1}) and $\Delta G^{\ddagger}$ (190 kJ mol^{-1}) values among all C−C cleavage steps in α-bound or α,β-bound intermediates (Figure 2, Table S1, structures in Figure 3A), but its λ value (2.5, $y = 3$, $l = 2$) is significantly smaller than measured values (4.0 ± 0.2). Isobutane activation via α- or α,β-bound intermediates would lead to values of λ (1.5−3) that are much smaller than those measured (4.0). These observations lead us to conclude that isobutane must activate via either α,γ- or α,β,γ-bound species.

Intermediates with α,γ-coordination to surfaces (e.g., $CH_2^*CH(CH_3)CH^*$) form by C−H activation at a $-CH_3$ group in $(CH_3)_2CHCH^*$. These species can undergo subsequent C−C bond cleavage via an α,β,γ-bound transition

DOI: 10.1021/acscatal.5b01950
ACS Catal. 2016, 6, 469−482

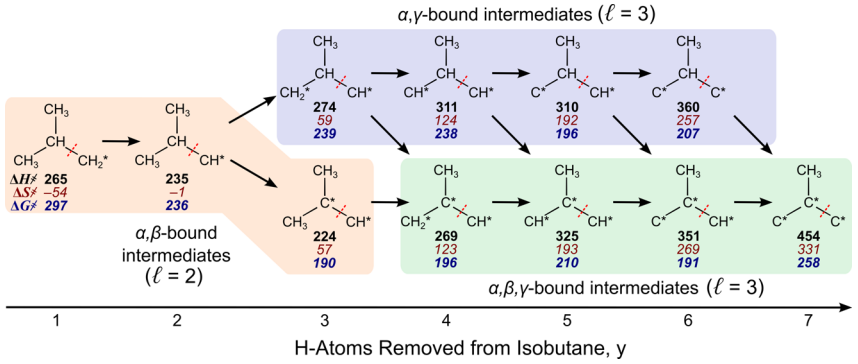

Figure 2. $\Delta H^{\ddagger}$ (black, bold), $\Delta S^{\ddagger}$ (red, italics), and $\Delta G^{\ddagger}$ (593 K, blue, bold italics) for the most favorable C−C cleavage reactions of various isobutane-derived intermediates. Site occupancies (l) are shown for C−C cleavage transition states for α,β-, α,γ-, and α,β,γ-bound intermediates.

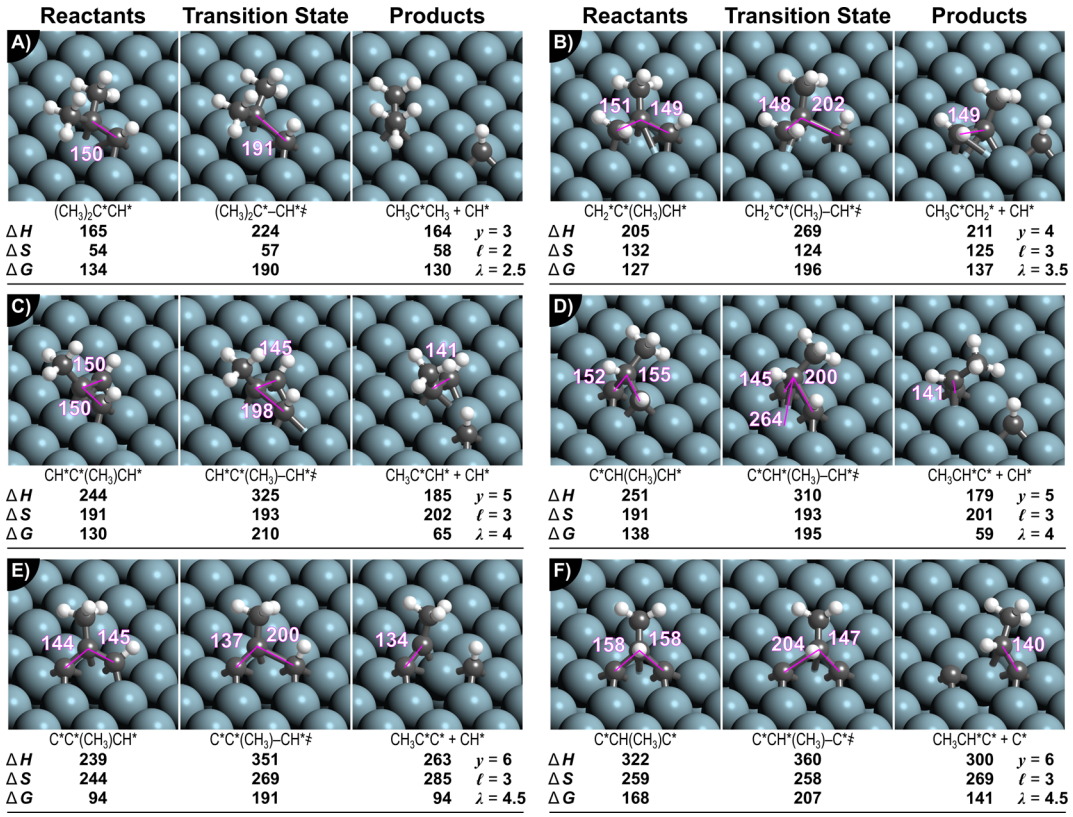

Figure 3. Reactant, product, and transition state structures for C−C cleavage of isobutane via (A) $(CH_3)_2C^*-CH^{*\ddagger}$, (B) $CH_2{}^*C^*(CH_3)-CH^{*\ddagger}$, (C) $CH^*C^*(CH_3)-CH^{*\ddagger}$, (D) $C^*CH^*(CH_3)-CH^{*\ddagger}$, (E) $C^*C^*(CH_3)-CH^{*\ddagger}$, and (F) $C^*CH^*(CH_3)-C^{*\ddagger}$. Enthalpies ($\Delta H$, kJ mol^{-1}), entropies (ΔS, J mol^{-1} K^{-1}) and free energies (ΔG, kJ mol^{-1}) for forming each state (and stoichiometric amounts of H_2) from isobutane and a H*-covered surface are shown. Notable C−C bond distances shown in pm.

state ($CH_2{}^*CH^*(CH_3)-CH^{*\ddagger}$). Although C−C bond rupture via $CH_2{}^*CH^*(CH_3)-CH^{*\ddagger}$ gives a $\Delta H^{\ddagger}$ value (274 kJ mol^{-1}) that is 39 kJ mol^{-1} larger than for $(CH_3)_2CH^*-CH^{*\ddagger}$ (235 kJ mol^{-1}, Figure 2), these $\Delta H^{\ddagger}$ differences are largely compensated by a concomitant increase in $\Delta S^{\ddagger}$ values (by 60 J mol^{-1} K^{-1}), rendering $\Delta G^{\ddagger}$ values for these two routes similar (236 and 239 kJ mol^{-1}) at 593 K. $CH_2{}^*CH(CH_3)CH^*$ intermediates can further dehydrogenate to form $CH^*CH(CH_3)CH^*$, which can undergo C−C bond cleavage via $CH^*CH(CH_3)-CH^{*\ddagger}$ transition states with a $\Delta H^{\ddagger}$ value of 311 kJ mol^{-1}. This $\Delta H^{\ddagger}$ is larger (by 37 kJ mol^{-1}) than for the route mediated by $CH_2{}^*CH^*(CH_3)-CH^{*\ddagger}$, but a similar compensation by a larger $\Delta S^{\ddagger}$ value (by 65 J mol^{-1} K^{-1}) leads once again to similar $\Delta G^{\ddagger}$ values (239 and 238 kJ mol^{-1}, respectively, 593 K; Figure 2) for $CH_2{}^*CH^*(CH_3)-CH^{*\ddagger}$ and $CH^*CH^*(CH_3)-CH^{*\ddagger}$. C−C cleavage mediated by $C^*CH(CH_3)-CH^{*\ddagger}$ (Figure 3D) has essentially the same $\Delta H^{\ddagger}$ value as that mediated by $CH^*CH(CH_3)-CH^{*\ddagger}$ but a larger $\Delta S^{\ddagger}$ (by 68 J mol^{-1} K^{-1}), leading to $\Delta G^{\ddagger}$ values (195 kJ mol^{-1}) that are smaller (by 43 kJ mol^{-1}) than those for $CH_2{}^*CH(CH_3)-CH^{*\ddagger}$ or $CH^*CH(CH_3)-CH^{*\ddagger}$ and which rank among the smallest $\Delta G^{\ddagger}$ values for isobutane activation (Figure 2). C−C cleavage via $C^*CH(CH_3)-C^{*\ddagger}$ (Figure 3F) has a slightly higher $\Delta G^{\ddagger}$ value (207 kJ mol^{-1}) than C−C cleavage via $C^*CH(CH_3)-C^{*\ddagger}$. Other C−C cleavages in α,γ-bound intermediates have larger $\Delta G^{\ddagger}$ (303−375 kJ mol^{-1}) than those shown in Figure 2 (196−239 kJ mol^{-1}), as shown in Figure 4 and Table S2. C−C cleavage via $C^*CH(CH_3)-CH^{*\ddagger}$

DOI: 10.1021/acscatal.5b01950
ACS Catal. 2016, 6, 469−482

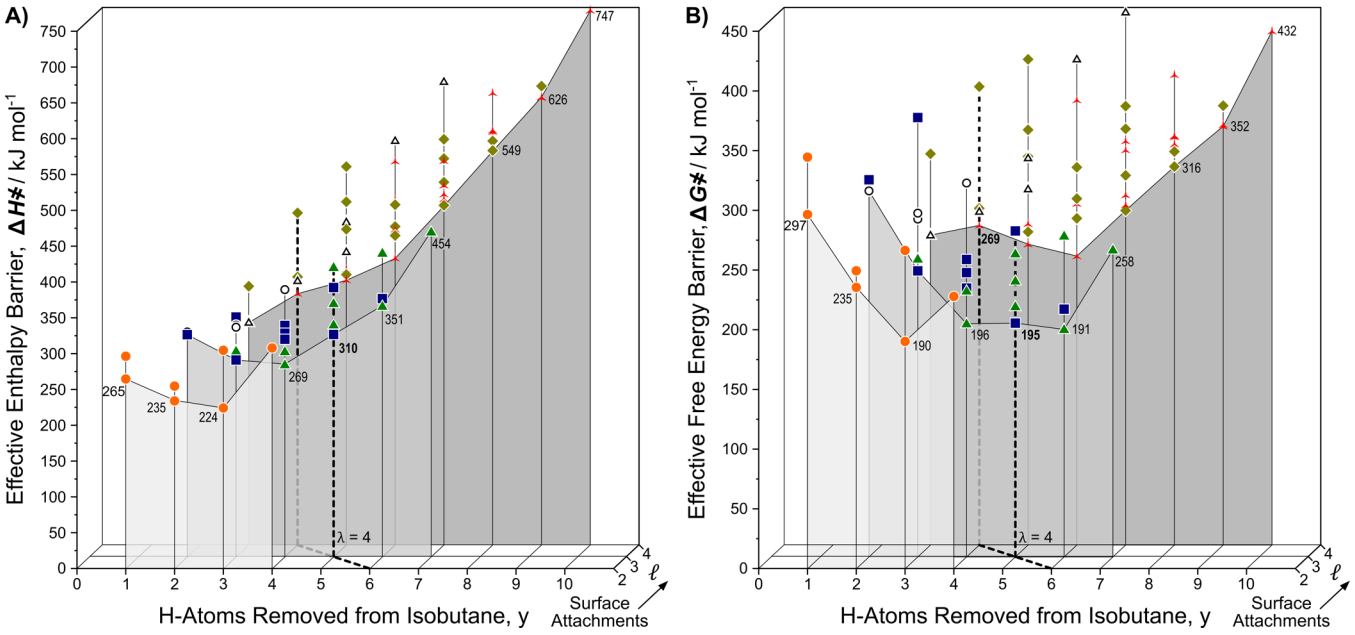

Figure 4. (A) $\Delta H^{\ddagger}$, and (B) $\Delta G^{\ddagger}$ (593 K, 1 bar H_2) for C−C bond activation routes in isobutane-derived intermediates via C−C cleavage in α,β-bound intermediates via $*CH_a-*CH_b(CH_3)_2^{\ddagger}$ (a = 0−3, b = 0−1) (●, orange) and $*CH_a*CH_b(CH_3)-CH_3*^{\ddagger}$ (a = 0−2, b = 0−1) (○) transition states; α,γ-bound intermediates via $*CH_aCH*(CH_3)-CH_b*^{\ddagger}$ (a = 0−2, b = 0−2) (■, blue); α,β,γ-bound intermediates via $*CH_aC*(CH_3)-CH_b*^{\ddagger}$ (a = 0−2, b = 0−2) (▲, green) and $*CH_aC*(CH_b*)-CH_3*^{\ddagger}$ (a = 0−2, b = 0−2) (Δ); α,γ,δ-bound intermediates via $*CH_aCH*(CH_c*)-CH_b*^{\ddagger}$ (a = 0−2, b = 0−2, c = 0−2) (♦, brown); $\alpha,\beta,\gamma,\delta$-bound intermediates via $*CH_aC*(CH_c*)-CH_b*^{\ddagger}$ (a = 0−2, b = 0−2, c = 0−2) (⅄, red). Tables S1−S5 in the SI show y, l, λ, ΔH_{act}, $\Delta H^{\ddagger}$, $\Delta S^{\ddagger}$, and $\Delta G^{\ddagger}$ for all transition states shown above. Color version (to add contrast between symbols) available online.

has the lowest $\Delta G^{\ddagger}$ (195 kJ mol^{-1}) among activations of α,γ-bound species, and it occurs without activation of the ^{3}C−H bond.

Dehydrogenation of $-CH_3$ groups in α,γ-bound intermediates forms α,γ,δ-bound species, such as $CH_2*CH(CH_2*)CH*$. Eighteen C−C activation steps of these α,γ,δ-bound intermediates were examined; C−C bonds cleave with $\Delta H^{\ddagger}$ values between 360 and 639 kJ mol^{-1} and $\Delta G^{\ddagger}$ values from 261 to 361 kJ mol^{-1} (Figure 4 and Table S3). These large $\Delta H^{\ddagger}$ and $\Delta G^{\ddagger}$ values show that these α,γ,δ-bound intermediates undergo C−C rupture at rates much lower than for α,β-coordinated $CH_3C*(CH_3)CH*$ intermediates, which can cleave C−C via $CH_3C*(CH_3)-CH*^{\ddagger}$ with $\Delta H^{\ddagger}$ and $\Delta G^{\ddagger}$ values of 224 and 190 kJ mol^{-1}, respectively.

Isobutane may also activate via α,β,γ-bound intermediates, after C−H activation at the ^{3}C atom in α,γ-bound intermediates, or via successive C−H activations of the $-CH_3$ group in α,β-bound $CH_3C*(CH_3)CH*$ (Figure 2). $\Delta H^{\ddagger}$ values increase from 224 to 351 kJ mol^{-1} with more extensive dehydrogenation of the $-CH_3$ group in routes mediated by $CH_x*C*(CH_3)-CH*^{\ddagger}$ transition states (from x = 0−3). The concomitant increases in $\Delta S^{\ddagger}$ values (caused by the evolution of a larger number of H_2 molecules) from 57 to 269 J mol^{-1} K^{-1} lead to $\Delta G^{\ddagger}$ values that are similar for activations via all transition states of the $CH_x*C*(CH_3)-CH*^{\ddagger}$ type (190 to 210 kJ mol^{-1} at 593 K, Figure 3B,C,E). C−C cleavage via $C*C*(CH_3)-C*^{\ddagger}$, however, has much larger $\Delta H^{\ddagger}$ (by 103 kJ mol^{-1}) and $\Delta G^{\ddagger}$ (by 67 kJ mol^{-1}) values than C−C cleavage via $C*C*(CH_3)-CH*^{\ddagger}$, reflecting the aversion toward producing atomic C* on Ir surfaces. $\Delta H^{\ddagger}$ (287 to 594 kJ mol^{-1}) and $\Delta G^{\ddagger}$ values (223 to 447 kJ mol^{-1}) for the 11 other possible C−C rupture pathways in α,β,γ-bound intermediates that were also calculated (Figure 4, Table S4) are much less stable than the C−C cleavage via α,β-bound $(CH_3)_2C*-CH*^{\ddagger}$ ($\Delta H^{\ddagger}$ of 224 and $\Delta G^{\ddagger}$ of 190 kJ mol^{-1}).

The cleavage of C−C bonds in $\alpha,\beta,\gamma,\delta$-bound intermediates was also examined (Figure 4, Table S5). They give $\Delta H^{\ddagger}$ values ranging from 352 to 747 kJ mol^{-1} and also large $\Delta G^{\ddagger}$ values (244−432 kJ mol^{-1}). These $\Delta H^{\ddagger}$ and $\Delta G^{\ddagger}$ values rule out activation routes involving $\alpha,\beta,\gamma,\delta$-bound intermediates, because of the much smaller $\Delta H^{\ddagger}$ and $\Delta G^{\ddagger}$ values for C−C activation routes mediated instead by $(CH_3)_2C*-CH*^{\ddagger}$ ($\Delta H^{\ddagger}$ and $\Delta G^{\ddagger}$ of 224 and 190 kJ mol^{-1}, respectively).

C−C bond cleavage via $CH_3C*(CH_3)-CH*^{\ddagger}$ has the lowest $\Delta H^{\ddagger}$ and $\Delta G^{\ddagger}$ values (224 and 190 kJ mol^{-1}, respectively) among the 71 distinct isobutane-derived intermediates examined (Figure 3b). The λ value for C−C bond cleavage via $CH_3C*(CH_3)-CH*^{\ddagger}$ (Figure 3A) is 2.5 (y = 3, l = 2), however, is much smaller than measured values (λ = 4.0 ± 0.2).[10] This comparison suggests that hydrogenolysis of isobutane may also cleave via other parallel pathways, whose $\Delta G^{\ddagger}$ values may be similar within uncertainties of our methods (e.g., for C−C rupture via $CH_2*C*(CH_3)-CH*^{\ddagger}$ (196 kJ mol^{-1}, Figure 3B), $CH*CH(CH_3)-CH*^{\ddagger}$ (195 kJ mol^{-1}, Figure 3D), and $C*C*(CH_3)-CH*^{\ddagger}$ (191 kJ mol^{-1}, Figure 3E) are similar to that via $CH_3C*(CH_3)-CH*^{\ddagger}$ (190 kJ mol^{-1}, Figure 3A). These four plausible routes involve transition states formed by removing 3−6 H atoms from isobutane (y) and bound on 2−3 exposed metal atoms (l), therefore, the resulting λ values range from 2.5 to 4.5 (measured λ = 4.0 ± 0.2), and thus their relative contributions differ with H_2 pressure (eq 4). C−C cleavage via $CH_3C*(CH_3)-CH*^{\ddagger}$ (λ = 2.5) has the highest DFT-predicted rate (eqs 4 and 7, 10 kPa isobutane, 593 K) at relevant H_2 pressures (1−20 bar), but its contribution ranges from ∼40% (1 bar H_2) to 98% (20 bar H_2), indicating that multiple pathways are present. The sum of DFT-predicted

DOI: 10.1021/acscatal.5b01950
ACS Catal. 2016, 6, 469−482

rates for all transition states in Figure 4 varied from 5.5×10^{-5} s^{-1} to 1.2×10^{-8} s^{-1} from 1 to 20 bar H_2, with a H_2-dependence consistent with a λ value of 2.8 (Figure 5),

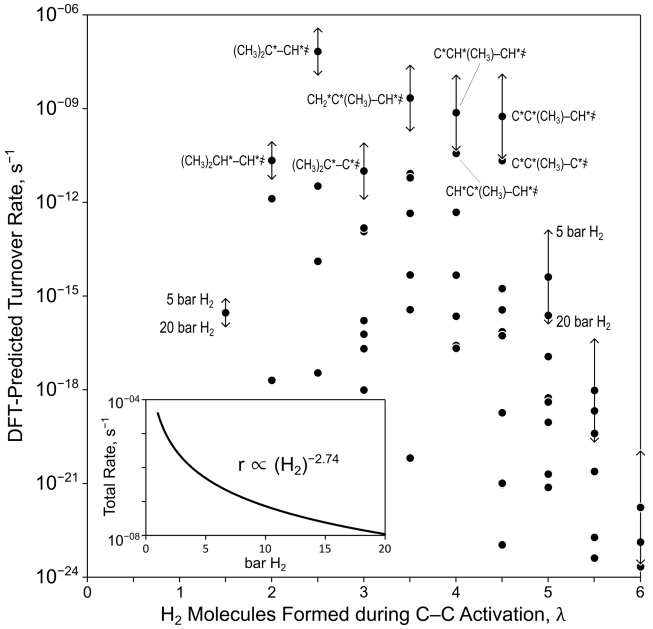

Figure 5. DFT-predicted hydrogenolysis rates (s^{-1}) for isobutane (10 kPa) cleavage via transition states shown in Figure 4 at 10 bar H_2, up/down arrows represent 5 and 20 bar H_2, respectively (the size of the bars depend only on λ, so they are omitted from most points for clarity. (Inset) Total rate of pathways from all 71 transition states from 1 to 20 bar H_2, showing a DFT-predicted λ value of 2.74.

significantly lower than measured values ($\lambda = 4.0 \pm 0.2$).[10] C–C cleavage via C*CH*(CH$_3$)–CH*‡ (Figure 3D) has a λ value of 4.0 and a $\Delta G^{\ddagger}$ (195 kJ mol^{-1}) comparable to that of CH$_3$C*(CH$_3$)–CH*‡ (190 kJ mol^{-1}, Figure 3A); these $\Delta G^{\ddagger}$ values are within the uncertainty associated with DFT methods, indicating that DFT alone cannot distinguish between these two pathways (Figure 3A and 3D) or others with similar $\Delta G^{\ddagger}$ values (Figure 3B and 3E). Measured λ values (4.0 ± 0.2) must then become the arbiter among these remaining plausible options; they indicate that C–C bonds cleave via C*CH*-(CH$_3$)–CH*‡ transition states ($\lambda = 4$, Figure 3D). The DFT-derived $\Delta H^{\ddagger}$ value for this route (310 kJ mol^{-1}) is larger than measured values (256 kJ mol^{-1}),[10] perhaps as a result of the neglected dispersive interactions in the DFT functionals used; such interactions stabilize the bound transition states but not the gaseous molecules or chemisorbed H atoms that determine $\Delta G^{\ddagger}$ (eq 9). DFT-predicted $\Delta S^{\ddagger}$ values (193 J mol^{-1} K^{-1}) for C–C cleavage via C*CH*(CH$_3$)–CH*‡, in contrast, agree with measured values (209 J mol^{-1} K^{-1}), because $\Delta S^{\ddagger}$ is predominantly determined by the entropy of gaseous molecules, which are unaffected by dispersive forces.

We conclude that ^{1}C–^{3}C bonds in isobutane cleave via α,γ-bound C*CH(CH$_3$)CH* species that cleave in a step mediated by C*CH*(CH$_3$)–CH*‡ (Figure 3D). These conclusions are based on the small $\Delta G^{\ddagger}$ value for this step and the agreement between the predicted and measured λ and $\Delta S^{\ddagger}$ values for isobutane hydrogenolysis on Ir surfaces nearly saturated with chemisorbed hydrogen.[10] The ^{3}C atom in C*CH(CH$_3$)CH* does not undergo C–H cleavage during C–C hydrogenolysis, and thus is not bound to the surface preceding C–C cleavage. The distance between the ^{3}C atom and the metal surface (264 pm) in the transition state is significantly longer than in the product state (240 pm), which are both significantly longer than ^{1}C–M bonds (210 pm) (Figure 3D). These long ^{3}C–M

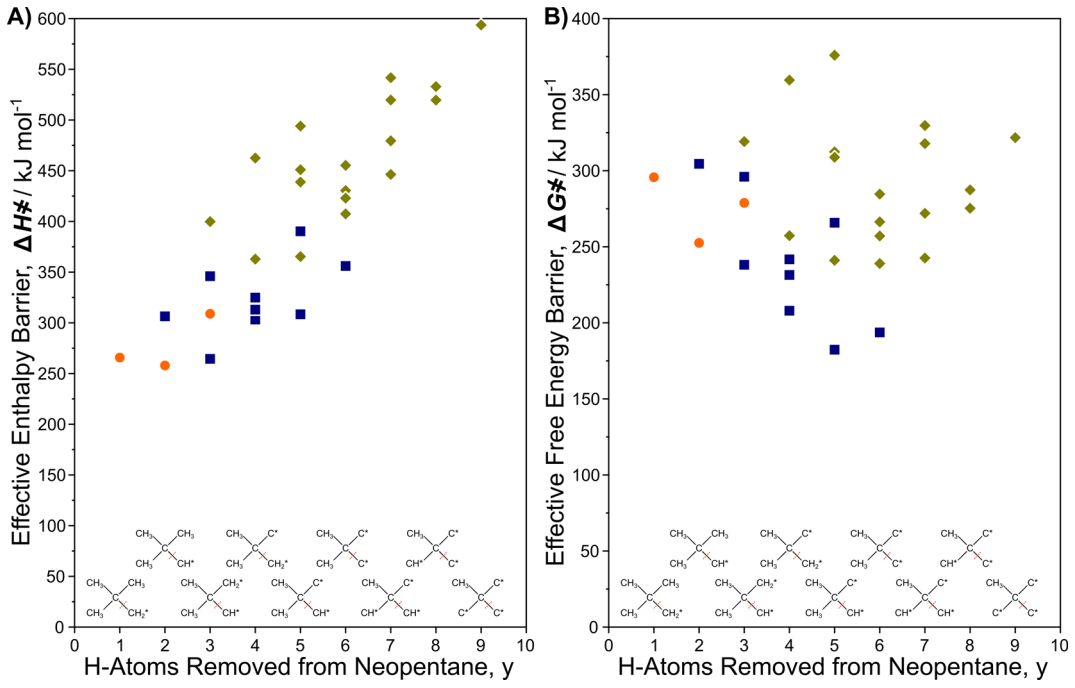

Figure 6. (A) $\Delta H^{\ddagger}$ and (B) $\Delta G^{\ddagger}$ for C–C bond activations of neopentane-derived intermediates via C–C activations of: α-bound intermediates (●, orange); α,γ-bound intermediates (■, blue); α,γ,δ-bound intermediates (♦, brown). The intermediate with the lowest $\Delta H^{\ddagger}$ and $\Delta G^{\ddagger}$ is shown near the ordinate for each number of H atoms removed from neopentane. Tables S2, S3, and S6 in the SI show y, I, λ, ΔH_{act}, $\Delta H^{\ddagger}$, $\Delta S^{\ddagger}$, and $\Delta G^{\ddagger}$ for all transition states shown above. Color version (to add contrast between symbols) available online.

DOI: 10.1021/acscatal.5b01950
ACS Catal. 2016, 6, 469–482

distances indicate that the metal surface interacts weakly with the ^{3}C atom upon C−C cleavage, in contrast to C−C cleavage of *n*-alkanes as further discussed in Section 3.4.

3.2. Neopentane Hydrogenolysis. Neopentane has four indistinguishable ^{4}C−^{1}C bonds and undergoes hydrogenolysis by cleaving these bonds to form methane and isobutane.[11,35,57−65] The ^{4}C atom lacks a H atom, thus precluding its dehydrogenation and binding, at least without intervening skeletal isomerization. Also, the presence of the ^{4}C atom requires that any H atoms removed from the CH_3 groups must lead to the formation of C-M bonds, because C═C cannot form. As a result, ^{4}C−^{1}C rupture in neopentane must occur via transition states that form from *α*-, *α,γ*-, or *α,γ,δ*-bound intermediates. We examine next the complete set of 30 distinct ^{4}C−^{1}C rupture transition states that can form from the 18 possible *α*-, *α,γ*-, or *α,γ,δ*-bound intermediates.

The three possible *α*-bound intermediates can undergo C−C cleavage via transition states that bind the ^{4}C atom to the surface at the $(CH_3)_3C^*-CH_x^{*‡}$ transition state after removing 1−3 H atoms from one CH_3 group (x = 0−2). These transition states have $\Delta H^‡$ values of 266, 258, and 309 kJ mol^{-1} for $-CH_2^*$, $-CH^*$, and $-C^*$ terminal groups in $(CH_3)_3C^*-CH_x^{*‡}$; these trends provide evidence for a significant enthalpy barrier when a C* moiety forms upon C−C cleavage, as also observed for C−C activation in *α*-bound *n*-alkanes[23] and isobutane. The $\Delta G^‡$ values for transition states with $-CH_2^*$, $-CH^*$, and $-C^*$ terminal groups show that $(CH_3)_3C^*-CH^{*‡}$ transition states mediate the most favorable path, with a $\Delta G^‡$ value (253 kJ mol^{-1}) that is smaller than for activation routes mediated by $(CH_3)_3C^*-CH_2^{*‡}$ or $(CH_3)_3C^*-C^{*‡}$ complexes (279 and 296 kJ mol^{-1}) (Figure 6, Table S6).

Neopentane-derived *α,γ*-bound intermediates can undergo C−C rupture via nine distinct transition states with the structure and stoichiometry of $CH_a^*C^*(CH_3)_2-CH_b^{*‡}$ (a = 0−2, b = 0−2); their DFT-derived $\Delta H^‡$ and $\Delta G^‡$ values are shown in Figure 6 and Table S2. C−C cleavage via a $CH^*C^*(CH_3)_2-CH^{*‡}$ (y = 5, l = 3, λ = 4) is the most favorable pathway; its $\Delta G^‡$ value of 182 kJ mol^{-1} is 11 kJ mol^{-1} lower than the next-lowest value (for C−C cleavage via $CH_2^*C^*(CH_3)_2-C^{*‡}$). The ^{4}C atom in $CH^*C^*(CH_3)_2-CH^{*‡}$ is weakly interacting with the metal surface (^{4}C−M distance of 276 pm in contrast to ^{1}C-M bonds 210 pm long), and this C−C cleavage is homologous to ^{3}C−^{1}C cleavage in isobutane via $CH^*CH^*(CH_3)-CH^{*‡}$ (Figure 3D), which involves a ^{3}C atom weakly interacting with the metal surface (^{3}C−M distance of 264 pm in the transition state).

Neopentane-derived *α,γ,δ*-bound intermediates $CH_a^*C^*(CH_b^*)(CH_3)-CH_c^{*‡}$ (a = 0−2, b = 0−2, c = 0−2) can undergo C−C rupture via 18 distinct transition states with structure and stoichiometry given by $CH_a^*C^*(CH_b^*)(CH_3)-CH_c^{*‡}$. Their $\Delta H^‡$ (368−604 kJ mol^{-1}) and $\Delta G^‡$ (239−375 kJ mol^{-1}) values (Table S3) are much larger than for C−C cleavage in the *α,γ*-bound intermediates described in the previous paragraph ($\Delta H^‡$ = 308 kJ mol^{-1}; $\Delta G^‡$ = 182 kJ mol^{-1}). Therefore, these *α,γ,δ*-bound intermediates are not likely to contribute to measured neopentane hydrogenolysis rates, as similar calculations have also indicated in the case of isobutane hydrogenolysis.

The $\Delta H^‡$ and $\Delta G^‡$ values for C−C cleavage mediated by the 30 neopentane-derived transition states are shown in Figure 6. C−C cleavage in *α,γ*-bound $C^*(CH_3)_2CCH^*$ via $C^*(CH_3)_2C^*-CH^{*‡}$ transition states proceeds with the lowest activation free energy barrier ($\Delta G^‡$ = 182 kJ mol^{-1}; Figure 6B; 593 K, 1 bar); the structure of this transition state is shown in Figure 7. The difference between its $\Delta G^‡$ value (182 kJ mol^{-1}, λ = 4) and that of the next most facile route (194 kJ mol^{-1} for C−C cleavage via $C^*(CH_3)_2C^*-C^{*‡}$, λ = 4.5) indicates that the *α,γ*-bound $C^*(CH_3)_2C^*-CH^{*‡}$ transition state accounts for the products formed in neopentane hydrogenolysis. This conclusion is supported by calculated rates (determined using eq 4 and DFT-predicted values of λ and $\Delta G^‡$) that are more than 10 times larger than for all other C−C cleavage transition states at >1 bar H_2 (Figure 8), thus accounting for the majority (>95%) of the total neopentane hydrogenolysis rate (593 K). In contrast, four distinct transition states for ^{1}C−^{3}C cleavage in isobutane gave similar $\Delta G^‡$ values (190−196 kJ mol^{-1}; Figure 3b), and therefore, the observed isobutane C−C hydrogenolysis rates contain comparable contributions from multiple pathways and give a reactivity-averaged value for λ (2.7). The

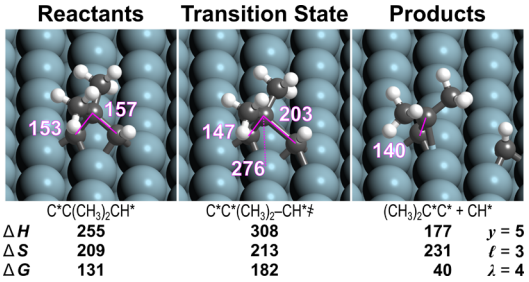

Figure 7. Reactant, product and transition state structures for C−C cleavage of neopentane via $C^*C^*(CH_3)_2-CH^*$. Enthalpies (kJ mol^{-1}), entropies (J mol^{-1} K^{-1}) and free energies (kJ mol^{-1}) for forming each state (and stoichiometric amounts of H_2) from neopentane and a H*-covered surface are shown. Notable C−C bond distances shown in pm.

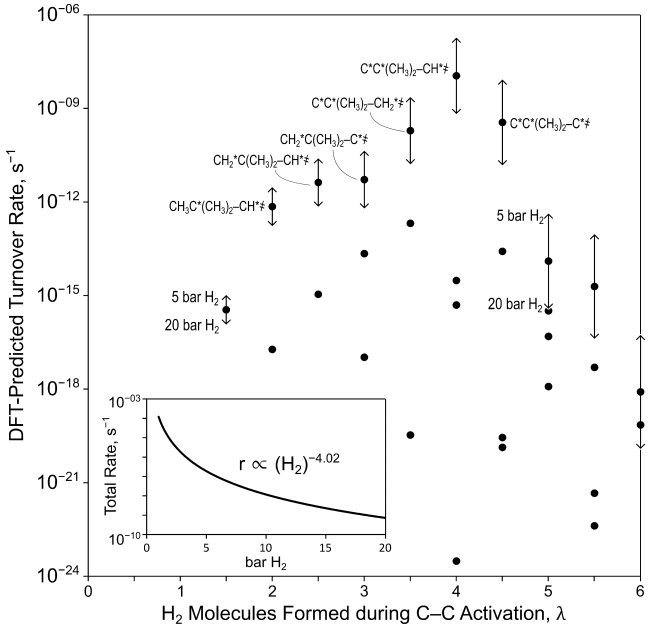

Figure 8. DFT-predicted hydrogenolysis rates (s^{-1}) for neopentane (10 kPa) cleavage via transition states shown in Figure 6 at 10 bar H_2, up/down arrows represent 5 and 20 bar H_2, respectively (the size of the bars depend only on λ, so they are omitted from most points for clarity. (Inset) Total rate across all 30 transition states from 1 to 20 bar H_2, showing a DFT-predicted λ value of 4.02.

DOI: 10.1021/acscatal.5b01950
ACS Catal. 2016, 6, 469−482

central ^{4}C atom in neopentane has no H atoms to lose, thus preventing the formation of α,β- or α,β,γ-bound intermediates that form and undergo C−C cleavage during isobutane hydrogenolysis.

3.3. 2,3-Dimethylbutane Hydrogenolysis. 2,3-Dimethylbutane contains a ^{3}C−^{3}C bond that cleaves at rates also described by eq 4 but with a λ value of 4.3 ± 0.3 (0.7 nm Ir clusters); these λ values are slightly larger than those measured for ^{3}C−^{1}C bond cleavage in isobutane (4.0 ± 0.2) or ^{1}C−^{1}C, ^{1}C−^{2}C, or ^{2}C−^{2}C bonds cleavage of *n*-alkanes (3.0 ± 0.2).[10,22,30] A λ value of 4.3 ± 0.3 is consistent with the combined removal of 8−9 H atoms from 2,3-dimethylbutane and the H*-saturated surface to form the kinetically relevant transition state. The ^{3}C−^{3}C bond being cleaved, however, contains only two H atoms, indicating that C−C activation of 2,3-dimethylbutane must occur after H-removal from ancillary C atoms with the concomitant formation of C−M bonds.

2,3-Dimethylbutane molecules can form 289 dehydrogenated intermediates (bound at 1−6 points at the surface through many combinations of C atoms, Figure 9). Such diversity of

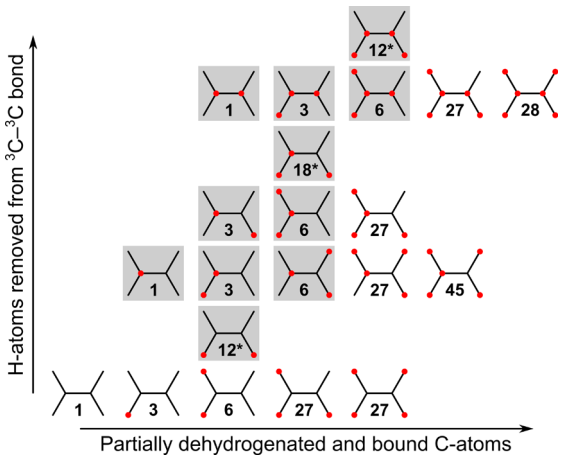

Figure 9. Forms of partially dehydrogenated 2,3-dimethylbutane intermediates. Dots indicate a C atom that has undergone C−H activation and is bound to the metal surface. Numbers within each backbone indicate the number of different intermediates with those surface attachments. Shaded sets indicate intermediates with homologues previously examined for *n*-alkane and/or isobutane activations. *Both cis and trans isomers are counted here, only the cis isomer is shown.

intermediates renders the full analysis of their energetics and reactivity inefficient and computationally arduous. These ^{3}C−^{3}C cleavages form C_3 intermediates on the Ir surface:

$$C_6H_{14} + lH^* \rightarrow C_3H_a^{la}* + C_3H_b^{lb}* + \lambda H_2 \quad (12)$$

and the complete set of C_3 intermediates have been isolated on Ir surfaces in previous work examining propane hydrogenolysis.[23] ^{3}C−^{3}C cleavage transition states are less stable than the product state shown in eq 12 (as reverse free energy barriers are ≥0 kJ mol^{-1}). Thus, we first calculate reaction enthalpies and free energies to form the C_3 products of ^{3}C−^{3}C cleavage and stoichiometric amounts of H_2 from 2,3-dimethylbutane (ΔH_P and ΔG_P):

$$\Delta H_P = H[C_3H_a^{la}*] + H[C_3H_b^{lb}*] + \lambda H[H_2] - H[C_6H_{14}] - lH[H^*] \quad (13)$$

$$\Delta G_P = G[C_3H_a^{la}*] + G[C_3H_b^{lb}*] + \lambda G[H_2] - G[C_6H_{14}] - lG[H^*] \quad (14)$$

which represent lower bounds for $\Delta H^{\ddagger}$ and $\Delta G^{\ddagger}$. ΔH_P values (Figure 10A) increase with increasing extents of dehydrogenation in reactive intermediates, such that the minimum ΔH_P value (98 kJ mol^{-1}) is for direct activation of 2,3-dimethylbutane, and this trend reflects the endothermic nature of C−H activations. ΔG_P values (Figure 10B), in contrast, reflect the entropic benefits associated with H_2 formation during quasi-equilibrated dehydrogenation and are smallest (and similar) for three intermediates which are formed from the removal of 6 H atoms from 2,3-dimethylbutane (14, 20, and 27 kJ mol^{-1} for C*CH(CH_3)CH(CH_3)C*, C*CH(CH_3)C*-(CH_3)CH*, and CH*C*(CH_3)C*(CH_3)CH*). The ΔG_P values for these isomeric intermediates increase from 14 to 27 kJ mol^{-1} as the number of C−M bonds increases from 2 to 4. The transition states for ^{3}C−^{3}C cleavage in these three intermediates were isolated (Figure 11) and cleavage steps mediated via C*CH*(CH_3)−CH*(CH_3)C*‡ complexes (y = 6, l = 4, λ = 5) gave the lowest $\Delta H^{\ddagger}$ (286 kJ mol^{-1}) and $\Delta G^{\ddagger}$ (119 kJ mol^{-1}) barriers. This $\Delta G^{\ddagger}$ barrier (119 kJ mol^{-1}) is lower than the ΔG_P values for 172 of the 289 distinct intermediates (Figure 10B), which therefore must exhibit $\Delta G^{\ddagger}$ barriers larger than for routes mediated by C*CH*(CH_3)−CH*(CH_3)C*‡; we conclude that such intermediates cannot significantly contribute to measured 2,3-dimethylbutane hydrogenolysis rates. The structures of all bound intermediates with ΔG_P values lower than 100 kJ mol^{-1} were determined and used to calculate reaction enthalpies and free energies for their formation (with stoichiometric amounts of H_2 from 2,3-dimethylbutane) (ΔH_R and ΔG_R).

$$C_6H_{14} + lH^* \rightarrow C_6H_{(14-y)}^{l}* + \lambda H_2 \quad (15)$$

$$\Delta H_R = H[C_6H_{(14-y)}^{l}*] + \lambda H[H_2] - H[C_6H_{14}] - lH[H^*] \quad (16)$$

$$\Delta G_R = G[C_6H_{(14-y)}^{l}*] + \lambda G[H_2] - G[C_6H_{14}] - lG[H^*] \quad (17)$$

These ΔH_R and ΔG_R values also represent the lower bounds for $\Delta H^{\ddagger}$ and $\Delta G^{\ddagger}$. ΔG_R values ranged from 16 to 302 kJ mol^{-1}, and 16 of them were smaller than 110 kJ mol^{-1} and transition states for ^{3}C−^{3}C cleavage were isolated for the C−C cleavage reactions of these 16 intermediates. In addition, 71 transition states for ^{3}C−^{3}C cleavage were isolated which share homologous transition states with isobutane or butane activations to determine the effects of branching on $\Delta H^{\ddagger}$ and $\Delta G^{\ddagger}$ values (to be presented separately).

$\Delta H^{\ddagger}$ and $\Delta G^{\ddagger}$ values for 80 ^{3}C−^{3}C cleavage reactions of 2,3-dimethylbutane are shown in Figure 12. Reactions occurring through α,β-bound (CH_3)$_2$C*C*(CH_3)$_2$ and α,δ-bound C*CH(CH_3)CH(CH_3)C* species have $\Delta H^{\ddagger}$ values of 284 and 286 kJ mol^{-1}; these $\Delta H^{\ddagger}$ values are much smaller than for all other ^{3}C−^{3}C cleavage reactions (≥307 kJ mol^{-1}). These α,β-bound and α,δ-bound (CH_3)$_2$C*−C*(CH_3)$_2^{\ddagger}$ transition states bind onto two sites (l = 2) and require that two H atoms be removed from 2,3-dimethylbutane (y = 2), thus leading to λ values (λ = 2), which are much smaller than measured values (4.3 ± 0.3) [10]. C*CH*(CH_3)−CH*(CH_3)C*‡ transition states (Figure 11A), in contrast, require four sites (l = 4) and

DOI: 10.1021/acscatal.5b01950
ACS Catal. 2016, 6, 469−482

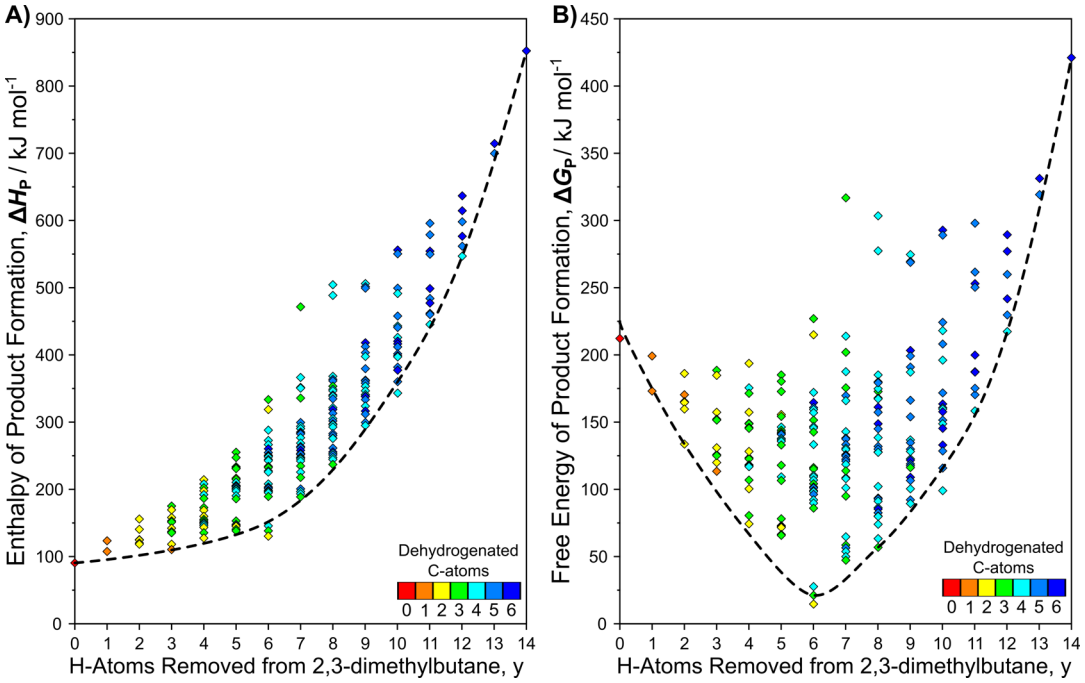

Figure 10. (A) Enthalpy and (B) free energy to form ^{3}C–^{3}C cleavage products (ΔH_P and ΔG_P) from 289 intermediates derived from 2,3-dimethylbutane. These ΔH_P and ΔG_P values represent lower-bounds for $\Delta H^{\ddagger}$ and $\Delta G^{\ddagger}$ for 2,3-dimethylbutane activation via these intermediates. The color of the symbol (in digital versions) represents the number of dehydrogenated C atoms (and thus attachments to the surface) and to prevent overlap, symbols are shifted based on the number of attachments.

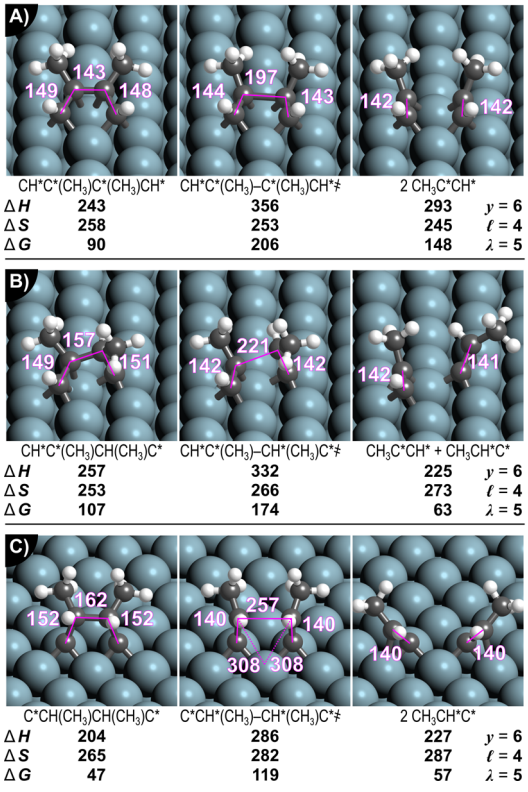

Figure 11. Reactant, product, and transition state structures for C–C cleavage of 2,3-dimethylbutane via (A) CH*C*(CH$_3$)–C*(CH$_3$)-CH*‡, (B) CH*C*(CH$_3$)–CH*(CH$_3$)C*‡, and (C) C*CH*(CH$_3$)–CH*(CH$_3$)C*‡. Enthalpies (kJ mol^{-1}), entropies (J mol^{-1} K^{-1}), and free energies (kJ mol^{-1}) for forming each state (and stoichiometric amounts of H_2) from 2,3-dimethylbutane and a H*-covered surface are shown. Notable C–C bond distances shown in pm.

the loss of six H atoms from 2,3-dimethylbutane, thus giving a λ value of 5, which is slightly larger than those measured (4.3 ± 0.3). These larger λ values also lead to much larger $\Delta S^{\ddagger}$ values for C*CH(CH$_3$)CH(CH$_3$)C* activation (283 J mol^{-1} K^{-1}) than for C*(CH$_3$)$_2$(CH$_3$)$_2$C* activation (−2 J mol^{-1} K^{-1}), which leads to $\Delta G^{\ddagger}$ values that are much smaller for C–C cleavage via C*CH*(CH$_3$)–CH*(CH$_3$)C* (119 kJ mol^{-1}) than for cleavage via (CH$_3$)$_2$C*–C*(CH$_3$)$_2$ (285 kJ mol^{-1}). This $\Delta G^{\ddagger}$ barrier for C*CH(CH$_3$)CH(CH$_3$)C*-mediated routes (119 kJ mol^{-1}) is also much smaller than for any other C–C cleavage route of 2,3-dimethylbutane-derived species (≥171 kJ mol^{-1}) (Figure 12), thus rendering all other routes kinetically irrelevant, as shown by rates several orders of magnitude higher for cleavage via C*CH*(CH$_3$)–CH*(CH$_3$)-C* at >1 bar H_2 and 593 K (Figure 13). 2,3-Dimethylbutane thus activates solely via C*CH(CH$_3$)CH(CH$_3$)C* activation, which gives a λ value of 5 at high H*-coverage if the transition state requires four sites.

The λ value for C*CH(CH$_3$)CH(CH$_3$)C*-mediated routes (5) is slightly larger than measured values (4.3 ± 0.3). DFT-derived $\Delta G^{\ddagger}$ values indicate a single dominant route for C–C cleavage pathways. Consequently, these differences in λ suggest that the relevant transition state displaces fewer than the four H atoms indicated by the number of C atoms bound in the product state. Such differences may reflect either C*CH*-(CH$_3$)–CH*(CH$_3$)C*‡ species that require fewer than four "sites" or that H* coverages are below 1 ML during 2,3-dimethylbutane hydrogenolysis even at H_2 pressures above 1 MPa in the experiments.[10] Neither ^{3}C atom in the cleaved ^{3}C–^{3}C bond is interacting with the metal surface in the C*CH*(CH$_3$)–CH*(CH$_3$)C*‡ transition state, as further discussed in Section 3.4, so just the two ^{1}C atoms are interacting strongly with the metal surface (Figure 11C), indicating that I may be two (instead of four). Rigorous

DOI: 10.1021/acscatal.5b01950
ACS Catal. 2016, 6, 469–482

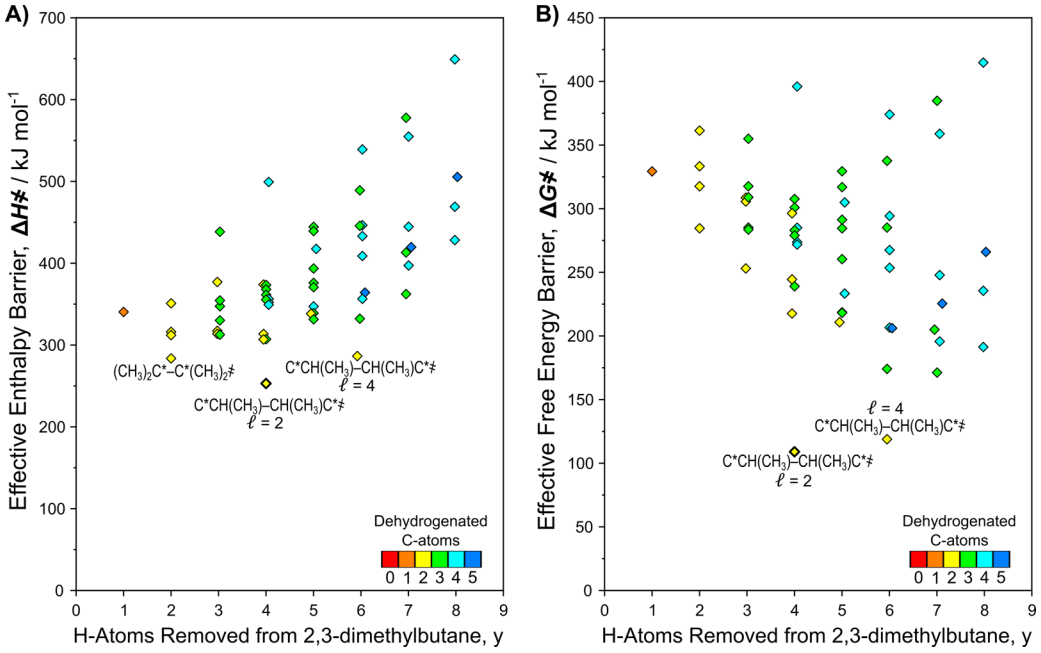

Figure 12. (A) $\Delta H^{\ddagger}$ and (B) $\Delta G^{\ddagger}$ values for $^{3}C-^{3}C$ cleavage if 2,3-dimethylbutane-derived intermediates. The color of the symbol (in online versions) represents the number of dehydrogenated C atoms (and thus attachments to the surface) and to prevent overlap, symbols are shifted based on the number of attachments. C−C cleavage of C*CH(CH_3)CH(CH_3)C* shown with a two-site (l = 2) and four-site (l = 4) transition state.

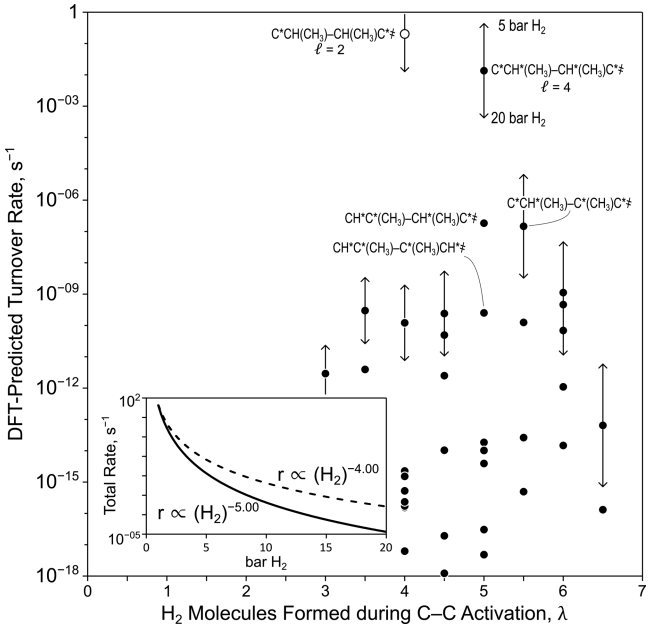

Figure 13. DFT-predicted hydrogenolysis rates (s^{-1}) for 2,3-dimethylbutane (10 kPa) cleavage via transition states shown in Figure 9 at 10 bar H_2, up/down arrows represent 5 and 20 bar H_2, respectively (the size of the bars depend only on λ, so they are omitted from most points for clarity. C−C cleavage of C*CH(CH_3)CH(CH_3)C* shown with a two-site (l = 2, open symbol) and four-site (l = 4) transition state. (Inset) Total rate from 1 to 20 bar H_2, showing a DFT-predicted λ value of 5.00 when l = 4 for C*CH*(CH_3)–CH*(CH_3)C*‡ or a λ of 4.00 when l = 2 for C*CH(CH_3)–CH(CH_3)C*‡ (dashed line).

determination of l requires calculating $\Delta G^{\ddagger}$ as a function of l on a fully covered H* Ir(111) surface and is outside of the scope of this work. A l value of 2 lowers the λ value predicted for activation via C*CH(CH_3)CH(CH_3)C* to 4, similar to the measured value of 4.3 ± 0.3. DFT-predicted $\Delta H^{\ddagger}$ depends on l (as H_2-desorption is endothermic) and varies from 286 kJ mol^{-1} (l = 4) to 253 kJ mol^{-1}) (l = 2); the latter of which is in good agreement with the measured value (257 kJ mol^{-1}).[10] Similarly, DFT-predicted $\Delta S^{\ddagger}$ (243 J mol^{-1} K^{-1}) and $\Delta G^{\ddagger}$ (109 kJ mol^{-1}) values (when l = 2) are also in good agreement with measured values ($\Delta S^{\ddagger}$ of 247 J mol^{-1} K^{-1} and $\Delta G^{\ddagger}$ of 111 kJ mol^{-1}), indicating that l = 2 for this reaction.

A l value of 2 indicates that the ^{3}C atoms directly involved in $^{3}C-^{3}C$ cleavage do not interact with the metal surface during transition-state formation, a C−C cleavage pathway very different from those described for activations of ethane[22] and larger n-alkane[30] which occur via α,β-coordinated (η^2, η^2) complexes in which both C atoms in the cleaved bond are strongly bound to the metal surface both prior to and in the C−C cleavage transition state. These two pathways for C−C cleavage are directly compared with charge analysis methods (QUAMBO)[66] in the following section.

3.4. C−C Bond Cleavage at or Away from Bound C Atoms: Contrasting *n*-Butane and 2,3-Dimethylbutane Hydrogenolysis. In this section, we examine the evolution of charge along the reaction coordinate in order to contrast the details of the cleavage of $^{2}C-^{2}C$ bonds within n-butane with that of $^{3}C-^{3}C$ bonds within 2,3-dimethylbutane. n-Butane and other n-alkanes undergo C−C cleavage after each of the C atoms in the C−C bond loses two H atoms and forms two C−M bonds, leading to the formation of RC*C*R′ intermediates that then cleave the C−C bond in the sole kinetically relevant step. C−C cleavage proceeds via RC*−C*R′‡ transition states in which each C atom in the cleaved bond binds at a 3-fold hollow site through three C−M bonds (Figure 14A) as two CH_3C^* species form. These RC*−C*R′‡ transition states require two sites on the Ir surface (λ = 3; y = 4, l = 2)).[20] The RC*C*R′ reactant state acquires 0.176 e^- from the Ir surface in forming this transition state, which, in turn, gains an additional 0.128 e^- as it forms the two CH_3C^* products (Figure 14A).

DOI: 10.1021/acscatal.5b01950
ACS Catal. 2016, 6, 469−482

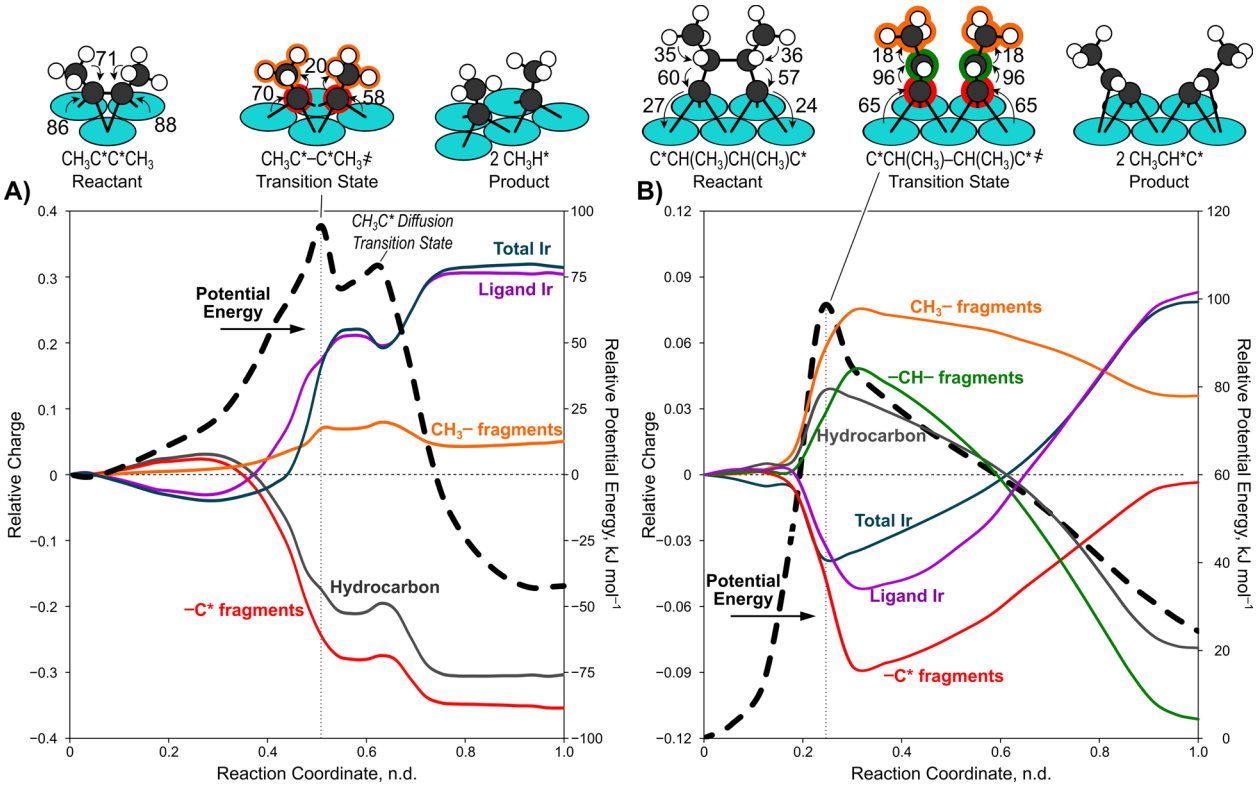

Figure 14. Reaction coordinate diagrams showing relative electronic energy (kJ mol^{-1} dashed lines) and charges (in e^-, solid lines) for C−C cleavage of (A) butane via $CH_3C^*-C^*CH_3^{\ddagger}$ and of (B) 2,3-dimethylbutane via $C^*CH(CH_3)-CH(CH_3)C^{*\ddagger}$ transition states. Total partial charge on the Ir surface shown in blue and that on Ir atoms directly bound to hydrocarbon fragments in pink (ligand Ir) in the online version. Furthermore, charges on the hydrocarbon are shown in gray, charges on the CH_3- fragments are shown in orange, those on the −C* fragments are shown in red, and those on the −CH− fragments are shown in green (for 2,3-dimethylbutane activation via $C^*CH(CH_3)-CH(CH_3)C^{*\ddagger}$). Above each plot are illustrations displaying reactant, transition state, and product structures as well as the charge transfer (in $e^- \times 10^3$) to/from the surface and between hydrocarbon fragments for each C−C cleavage reaction.

Table 1. Effects of C-Atom Substitution on C−C Cleavage Mechanisms

			^{x}C atom leaves alkane chains in			
alkane			^{1}C	^{2}C	^{3}C	^{4}C
ethane	^{1}C−^{1}C	→	2 CH*	—	—	—
propane, butane	^{1}C−^{2}C	→	CH*	RC*	—	—
isobutane	^{1}C−^{3}C	→	CH*	—	RCH*C*	—
neopentane	^{1}C−^{4}C	→	CH*	—	—	RC*R′C*
ethane	^{1}C−^{1}C	→	2 CH*	—	—	—
butane	^{2}C−^{2}C	→	—	2 RC*	—	—
2,3-dimethylbutane	^{3}C−^{3}C	→	—	—	2 RCH*C*	—

This monotonic transfer of charge from the metal to the organic moiety is reminiscent of that observed in metal-atom-insertion reactions;[20] in these reactions, bonds cleave via electron donation from the metal atom into the antibonding orbitals of reactants as C−M bonds form. These *n*-butane hydrogenolysis pathways are common to all *n*-alkanes that contain only ^{1}C- and ^{2}C atoms (e.g., ethane, Figure S2).

The evolution of charge differs markedly for ^{3}C−^{3}C bond cleavage steps in 2,3 dimethylbutane. C−C cleavage occurs after all H atoms are removed from one of the ^{1}C atoms vicinal to each ^{3}C atom in the ^{3}C−^{3}C bond (at α,δ positions of the 2,3-dimethylbutane), which then bind onto 3-fold surface sites (Figure 11C, 14B). The two ^{3}C atoms do not lose their H atom or bind to the Ir surface and the ^{3}C−^{3}C bond cleaves without contact between each of its ^{3}C atoms and the metal surface; these ^{3}C atoms reside more than 308 pm away from the nearest Ir atom at the transition state. These ^{3}C−^{3}C cleavage steps involve electron transfer into the metal as the $C^*CH(CH_3)-CH(CH_3)C^*$ species form the transition state (Figure 14B), in contrast with the findings for ^{2}C−^{2}C bond cleavage in *n*-butane. The evolution of charge for ^{3}C−^{3}C cleavage is not monotonic along the reaction coordinate; the formation of the $C^*CH-(CH_3)-CH(CH_3)C^{*\ddagger}$ transition state involves the transfer of 0.051 e^- into the metal, while its decomposition into two $CH_3CH^*C^*$ moieties removes 0.130 e^- from the metal. The total charge on the two −CH− groups is +0.14 e^- at the $C^*CH(CH_3)-CH(CH_3)C^{*\ddagger}$ transition state. Similar pathways and intermediates are involved in ^{1}C−^{3}C cleavage in isobutane and ^{1}C−^{4}C cleavage in neopentane (Figures 3 and 7). The positive charge and sp^2-like geometry of the ^{3}C atoms (and ^{4}C

DOI: 10.1021/acscatal.5b01950
ACS Catal. 2016, 6, 469−482

atoms) during the cleavage of highly substituted bonds are reminiscent of carbenium-like C atom centers. The higher degree of substitution on these C atoms prevents the formation of two C−M bonds (thus preventing the coordination preferred by ethane (and other *n*-alkanes)) and provides stable carbenium-like intermediates that facilitate this novel C−C cleavage mechanism for ^{3}C−^{3}C activation in 2,3-dimethylbutane.

Theoretical treatments of the activation of ^{1}C−^{1}C, ^{1}C−^{2}C, ^{1}C−^{3}C, ^{1}C−^{4}C, and ^{2}C−^{2}C bonds in linear[22,23] and branched alkanes (this study) lead to some important guidance and broadly applicable concepts about the essential requirements for H-removal (and C−M bond formation) before C−C cleavage in alkanes. These are discussed next with the assistance from the entries in Table 1, which show the intermediates formed by C atoms of varying substitution upon C−C cleavage. ^{1}C- and ^{2}C atoms (present in ^{1}C−^{1}C, ^{1}C−^{2}C, ^{2}C−^{2}C, ^{1}C−^{3}C, and ^{1}C−^{4}C bonds) lose two H atoms before C−C cleavage, resulting in two C−M bonds and thus forming CH* or RC* intermediates upon decomposition of the C−C cleavage transition state (Table 1). These mechanistic conclusions for the cleavage of a variety of C−C bonds lead us to infer that ^{1}C- and ^{2}C atoms will always form CH* or RC* intermediates upon C−C cleavage, irrespective of the degree of substitution at the other C atom in the cleaved C−C bond. The evolution of charge during C−C cleavage in ethane (Figure S2) and butane (Figure 14) shows that electrons transfer from the metal surface into antibonding C−C orbitals as the C−M bonds form at these ^{1}C and ^{2}C atoms during C−C cleavage. ^{3}C and ^{4}C atoms (present in ^{1}C−^{3}C, ^{1}C−^{4}C, and ^{3}C−^{3}C bonds), in contrast to ^{1}C- and ^{2}C atoms, do not lose any H atoms before C−C cleavage. Instead, ^{1}C atoms vicinal to the ^{3}C and ^{4}C atoms lose all of their H atoms as these bonds are cleaved in isobutane, neopentane, and 2,3-dimethylbutane to form RCH*C* or RC*R′C* products in the C−C cleavage elementary step (Table 1). The loss of three H atoms from ^{1}C atoms vicinal to the C−C bond increases the $\Delta S^{\ddagger}$ (through the evolution of H_2 molecules) and connects ^{3}C- and ^{4}C atoms through C−C bonds to the metal surface. These indirect linkages allow charge to delocalize in ^{3}C and ^{4}C atoms, which adopt carbenium-like properties, such as a net positive charge and sp^2-like geometry (Figure 14), at their C−C cleavage transition states. These mechanistic considerations, supported by theory and experiment, lead to consistent trends and to predictive and general guidance for the effects of substitution on the rates, activation energies, and H_2 inhibition effects for *n*-alkanes and isoalkanes. These concepts are expected to extend to cycloalkanes, for which mechanistic resemblance to acyclic alkanes has been clearly established.[10,36]

4. CONCLUSIONS

Hydrogenolysis of ^{1}C−^{1}C and ^{1}C−^{2}C bonds of *n*-alkanes proceed via C−C cleavage of α,β-bound (η^2, η^2) RC*C*R′ intermediates. These transition states require two sites on the catalyst surface and have four fewer H atoms than their *n*-alkane reagents, resulting in three H_2 molecules formed with each transition state formation. This formation of H_2 leads to rates inhibited by $(H_2)^3$, and such a dependence is observed for ^{1}C−^{1}C and ^{1}C−^{2}C bond cleavage of *n*-alkanes, branched alkanes, and cycloalkanes. Bonds of branched species (such as isobutane or 2,3-dimethylbutane) containing ^{3}C atoms, however, cannot form these α,β-bound (η^2, η^2) RC*C*R′ intermediates. These species sacrifice additional H atoms in the form of C−H activations at ^{1}C atoms vicinal to the bond being broken, resulting in an increase in entropy, which decreases free energies for transition state formation and leads to greater inhibition by H_2 (rates proportional to $(H_2)^{-4}$ for isobutane and $(H_2)^{-4.3}$ for 2,3-dimethylbutane hydrogenolysis).[10] Isobutane and neopentane form α,γ-bound (η^3, η^2) C*C(CH_3)-(R)CH* intermediates which C−C cleave via form C*C*-(CH_3)(R)−CH*‡ transition states. 2,3-Dimethylbutane forms α,δ-bound (η^3, η^3) C*CH(CH_3)CH(CH_3)C* which cleaves C−C via C*CH*(CH_3)−CH*(CH_3)C*‡ transition states. These α,γ- and α,δ-bound transition states are consistent with increased H_2 inhibition for hydrogenolysis of branched species[10] and involve C−C activations in which one or both C atoms are not bound to the surface prior to cleavage (and either interact weakly or do not interact with the surface during C−C activation), in direct contrast with observations from *n*-alkane hydrogenolysis.

■ ASSOCIATED CONTENT

Supporting Information

The Supporting Information is available free of charge on the ACS Publications website at DOI: 10.1021/acscatal.5b01950.

Details of DFT calculations, including data tables with extended information for all computed reactions, a comparison of results with the PBE functional, and charge analysis for ethane activation via CH*CH* species (PDF)

■ AUTHOR INFORMATION

Corresponding Author

*E-mail: iglesia@berkeley.edu.

Notes

The authors declare no competing financial interest.

■ ACKNOWLEDGMENTS

The authors acknowledge Dr. Elif Gurbuz for helpful discussions and Dr. Craig Plaisance for the implementation of QUAMBO methods into VASP. Computational resources provided by the Molecular Science Computing Facility (MSCF) in the William R. Wiley Environmental Molecular Sciences Laboratory, a national scientific user facility sponsored by the U.S. Department of Energy, Office of Biological and Environmental Research at the Pacific Northwest National Laboratory, under proposal 47800.

■ REFERENCES

(1) Weitkamp, J.; Jacobs, P. A.; Martens, J. A. *Appl. Catal.* **1983**, *8*, 123−141.

(2) McVicker, G. B.; Daage, M.; Touvelle, M. S.; Hudson, C. W.; Klein, D. P.; Baird, W. C.; Cook, B. R.; Chen, J. G.; Hantzer, S.; Vaughan, D. E. W.; Ellis, E. S.; Feeley, O. C. *J. Catal.* **2002**, *210*, 137−148.

(3) Do, P. T.; Alvarez, W. E.; Resasco, D. E. *J. Catal.* **2006**, *238*, 477−488.

(4) Shi, H.; Gutierrez, O. Y.; Haller, G. L.; Mei, D.; Rousseau, R.; Lercher, J. A. *J. Catal.* **2013**, *297*, 70−78.

(5) Shi, H.; Li, X.; Haller, G. L.; Gutierrez, O. Y.; Lercher, J. A. *J. Catal.* **2012**, *295*, 133−145.

(6) Weisang, F.; Gault, F. G. *J. Chem. Soc., Chem. Commun.* **1979**, 519−520.

DOI: 10.1021/acscatal.5b01950
ACS Catal. 2016, 6, 469−482

(7) Speight, J. G. In *Kirck-Othmer Encyclopedia of Chemical Technology*; Kirk, R. E., Othmer, D. F., Eds.; John Wiley and Sons, Inc: New York, 2012; pp 1−49.
(8) Iglesia, E.; Reyes, S. C.; Madon, R. J.; Soled, S. L. *Adv. Catal.* **1993**, *39*, 221−302.
(9) Bond, G. C. *Metal-Catalysed Reactions of Hydrocarbons*; Springer: NewYork, 2005.
(10) Flaherty, D. W.; Hibbitts, D. D.; Iglesia, E. *J. Am. Chem. Soc.* **2014**, *136*, 9664−9676.
(11) Foger, K.; Anderson, J. R. *J. Catal.* **1979**, *59*, 325−339.
(12) Gault, F. G. *Adv. Catal.* **1981**, *30*, 1−95.
(13) Cimino, A.; Boudart, M.; Taylor, H. *J. Phys. Chem.* **1954**, *58*, 796−800.
(14) Kemball, C.; Taylor, H. S. *J. Am. Chem. Soc.* **1948**, *70*, 345−351.
(15) Morikawa, K.; Benedict, W. S.; Taylor, H. S. *J. Am. Chem. Soc.* **1936**, *58*, 1795−1800.
(16) Sinfelt, J. H. *Adv. Catal.* **1973**, *23*, 91−119.
(17) Gault, F. G. *C. R. Hebd. Seances. Acad. Sci.* **1957**, *245*, 1620.
(18) Maire, G.; Plouidy, G.; Prudhomme, J. C.; Gault, F. G. *J. Catal.* **1965**, *4*, 556−569.
(19) Kua, J.; Faglioni, F.; Goddard, W. A. *J. Am. Chem. Soc.* **2000**, *122*, 2309−2321.
(20) Chorkendorff, I.; Niemantsverdriet, J. W. *Concepts of Modern Catalysis and Kinetics*, 2nd ed.; Wiley-VCH: Weinheim, 2007.
(21) Sinfelt, J. H.; Taylor, W. F.; Yates, D. J. C. *J. Phys. Chem.* **1965**, *69*, 95−101.
(22) Flaherty, D. W.; Hibbitts, D. D.; Gürbuz, E. I.; Iglesia, E. *J. Catal.* **2014**, *311*, 350−356.
(23) Hibbitts, D. D.; Flaherty, D. W.; Iglesia, E., unpublished results.
(24) Cortright, R. D.; Watwe, Rm. M.; Spiewak, B. E.; Dumesic, J. A. *Catal. Today* **1999**, *53*, 395−406.
(25) Watwe, R. M.; Cortright, R. D.; Norskov, J. K.; Dumesic, J. A. *J. Phys. Chem. B* **2000**, *104*, 2299−2310.
(26) Zhao, Z.-J.; Moskaleva, L. V.; Rösch, N. *J. Catal.* **2012**, *285*, 124−133.
(27) Zhao, Z.-J.; Moskaleva, L. V.; Rösch, N. *J. Catal.* **2013**, *299*, 146−149.
(28) Zhao, Z.-J.; Moskaleva, L. V.; Rösch, N. *ACS Catal.* **2013**, *3*, 196−205.
(29) Cortright, R. D.; Watwe, R. M.; Dumesic, J. A. *J. Mol. Catal. A: Chem.* **2000**, *163*, 91−103.
(30) Flaherty, D. W.; Iglesia, E. *J. Am. Chem. Soc.* **2013**, *135*, 18586−18599.
(31) Sinfelt, J. H.; Yates, D. J. C. *J. Catal.* **1967**, *8*, 82−90.
(32) Engstrom, J. R.; Goodman, D. W.; Weinberg, W. H. *J. Am. Chem. Soc.* **1988**, *110*, 8305−8319.
(33) Bond, G. C.; Cunningham, R. H. *J. Catal.* **1997**, *166*, 172−185.
(34) Bond, G. C.; Slaa, J. C. *J. Mol. Catal. A: Chem.* **1996**, *106*, 135−149.
(35) Boudart, M.; Ptak, L. D. *J. Catal.* **1970**, *16*, 90−96.
(36) Flaherty, D. W.; Uzun, A.; Iglesia, E. *J. Phys. Chem. C* **2015**, *119*, 2597−2613.
(37) Yang, M.; Somorjai, G. A. *J. Am. Chem. Soc.* **2004**, *126*, 7698−7708.
(38) Weiss, M. J.; Hagedorn, C. J.; Mikesell, P. J.; Little, R. D.; Weinberg, W. H. *J. Am. Chem. Soc.* **1998**, *120*, 11812−11813.
(39) Dowie, R. S.; Whan, D. A.; Kemball, C. *J. Chem. Soc., Faraday Trans. 1* **1972**, *68*, 2150−2162.
(40) Kemball, C. *Catal. Rev.* **1971**, *5*, 23−53.
(41) Kemball, C.; Brown, R. *J. Chem. Soc., Chem. Commun.* **1987**, 771−773.
(42) Anderson, J. R. In *Advances in Catalysis*; EleyD. D., Weisz, P. B., Eds.; Elsevier: Amsterdam, 1973; Vol. *23*, pp 1−90.
(43) Kresse, G.; Furthmuller, J. *Comput. Mater. Sci.* **1996**, *6*, 15−50.
(44) Kresse, G.; Furthmuller, J. *Phys. Rev. B: Condens. Matter Mater. Phys.* **1996**, *54*, 11169−11186.
(45) Kresse, G.; Hafner, J. *Phys. Rev. B: Condens. Matter Mater. Phys.* **1993**, *47*, 558−561.
(46) Kresse, G.; Hafner, J. *Phys. Rev. B: Condens. Matter Mater. Phys.* **1994**, *49*, 14251−14269.
(47) Blochl, P. E. *Phys. Rev. B: Condens. Matter Mater. Phys.* **1994**, *50*, 17953−17979.
(48) Kresse, G.; Joubert, D. *Phys. Rev. B: Condens. Matter Mater. Phys.* **1999**, *59*, 1758−1775.
(49) Hammer, B.; Hansen, L.; Norskov, J. K. *Phys. Rev. B: Condens. Matter Mater. Phys.* **1999**, *59*, 7413−7421.
(50) Perdew, J.; Burke, K.; Ernzerhof, M. *Phys. Rev. Lett.* **1996**, *77*, 3865−3868.
(51) Zhang, Y.; Yang, W. *Phys. Rev. Lett.* **1998**, *80*, 890.
(52) Monkhorst, H. J.; Pack, J. D. *Phys. Rev. B* **1976**, *13*, 5188−5192.
(53) Singh, H. P. *Acta Crystallogr., Sect. A: Cryst. Phys., Diffr., Theor. Gen. Crystallogr.* **1968**, *24*, 469−471.
(54) Henkelman, G.; Jonsson, H. A. *J. Chem. Phys.* **2000**, *113*, 9978−9985.
(55) Jonsson, H. A.; Mills, G.; Jacobsen, K. W. In *Classical and Quantum Dynamics in Condensed Phase Simulations*; Berne, B. J., Ciccotti, G., Coker, D. F., Eds.; World Scientific: Singapore, 1998; p 385.
(56) Henkelman, G.; Jonsson, H. A. *J. Chem. Phys.* **1999**, *111*, 7010−7022.
(57) Childers, D.; Saha, A.; Schweitzer, N.; Rioux, R. M.; Miller, R.; Meyer, R. *ACS Catal.* **2013**, *3*, 2487−2496.
(58) Balakrishnan, K.; Schwank, J. *J. Catal.* **1991**, *132*, 451−464.
(59) Juszczyk, W.; Lomot, D.; Karpinski, Z.; Pielaszek, J. *J. Catal.* **1978**, *54*, 318.
(60) Juszczyk, W.; Karpinski, Z. *J. Catal.* **1989**, *117*, 519−532.
(61) Juszczyk, W.; Karpinski, Z.; Ratajczykowa, I.; Stanasiuk, Z.; Zielinski, J.; Sheu, L. L.; Sachtler, W. M. H. *J. Catal.* **1989**, *120*, 68−77.
(62) Botman, M. J. P.; Devreugd, K.; Zandbergen, H. W.; Deblock, R.; Ponec, V. *J. Catal.* **1989**, *116*, 467−479.
(63) Akhmedov, V. M.; Al-Khowaiter, S. H. *Catal. Rev.: Sci. Eng.* **2007**, *49*, 33−139.
(64) Ciapetta, F. G.; Wallace, D. N. *Catal. Rev.: Sci. Eng.* **1972**, *5*, 67−158.
(65) Anderson, J. R.; Avery, N. R. *J. Catal.* **1966**, *5*, 446−463.
(66) Qian, X.; Li, J.; Qi, L.; Wang, C.-Z.; Chan, T.-L.; Yao, Y.-X.; Ho, K.-M.; Yip, S. *Phys. Rev. B: Condens. Matter Mater. Phys.* **2008**, *78*, 245112.

DOI: 10.1021/acscatal.5b01950
ACS Catal. 2016, 6, 469−482